DETERMINATION OF RESIDUAL STRESS AND THERMAL BEHAVIOR FOR COMPOSITE LAMINATES

By

WILLIAM A. SCHULZ

A THESIS PRESENTED TO THE GRADUATE SCHOOL
OF THE UNIVERSITY OF FLORIDA IN PARTIAL FULFILLMENT
OF THE REQUIREMENTS FOR THE DEGREE OF
MASTER OF SCIENCE

UNIVERSITY OF FLORIDA

2005

ACKNOWLEDGMENTS

I would like to thank my advisor and supervisory committee chair (Dr. Peter Ifju) as well as my other committee members (Dr. Raphael Haftka and Dr. Bhavani Sankar) for their support, direction and advice. I want to give my gratitude to fellow assistants and true friends, Dr. Leishan Chen, Ryan Karkkainen, Donald Myers, Thomas Singer, and Lucian Speriatu, for their assistance in my efforts. A special thank you goes to Dr. Paul Hubner for his invaluable LABview programming advice. Special thanks also go to Dr. Theodore Johnson for his guidance and experience and Ron Brown for his machining expertise.

Finally, I would like to thank; my parents Bill and Diane; sister Amber; fiancée Jessica; as well as all of my family and friends for their love, support, and everything they have done for me.

TABLE OF CONTENTS

LIST OF TABLES

LIST OF FIGURES

LIST OF SYMBOLS AND ABBREVIATIONS

x-y	Coordinate system aligned with laminate 0º (x) and 90º (y) directions
1-2	Coordinate system aligned with lamina fiber (1) and transverse (2) directions
A	1st quadrant of laminate stiffness matrix, 3x3
CTE_x	Coefficient of thermal expansion in the x-direction
CTE_y	Coefficient of thermal expansion in the y-direction
E_1	Lamina elastic modulus in fiber direction
E_2	Lamina elastic modulus in transverse direction
G_{12}	Lamina shear modulus
N_x	Number of fringes in x-direction
N_y	Number of fringes in y-direction
N	Applied force per unit length vector, 3x1
N^M	Mechanical force per unit length vector, 3x1
N^T	Thermal force per unit length vector, 3x1
N^C	Chemical force per unit length vector, 3x1
NL	Number of layers in laminate
Q	Ply stiffness matrix
R	Reuter transformation matrix between engineering and tensorial strains, 3x3
T	Temperature
T_{test}	Specific temperature of test/prediction
T_{cure}	Peak temperature of composite cure cycle

ΔT Temperature difference of (Ttest-Tcure)

U Horizontal displacement

V Vertical displacement

α Experimentally measured CTE

α_{ave} Average laminate CTE

ε_x Strain in the x-direction

ε_y Strain in the y-direction

$\varepsilon_{apparent}$ Apparent measured strain from a strain gage, 3x1

ε_{CLT} Classical Laminate Theory predicted strain

ε_{chem} Chemical shrinkage vector of a unidirectional panel, 3x1

$\varepsilon_{gage\ foil\ expansion}$ Strain due to expansion/contraction of the strain gage itself, 3x1

ε_{lam} Laminate strain vector in x-y system, 3x1

$\varepsilon_{measured\ on\ reference}$ Strain measured from the reference strain gage, 3x1

ε_{res} Laminate residual strain vector in 1-2 system, 3x1

$\varepsilon_{thermo\text{-}mechanical}$ True strain on substrate due to thermal and mechanical loading, 3x1

$\varepsilon_{theoretical}$ Theoretical expansion of the reference material, 3x1

ε_{true} True strain on substrate due to thermal and mechanical loadings, 3x1

ε_{uni} Strain vector on a unidirectional panel in the x-y system, 3x1

ε_0 Laminate strain vector in x-y system measured at mid-plane, 3x1

f Frequency of reference diffraction grating

k Ply number index

τ Transformation matrix, 3x3

θ Angle between x-y and 1-2 coordinate systems

σ_{res} Residual stress vector in the 1-2 coordinate system, 3x1

t Ply thickness

v_{12} Lamina Poisson's ratio.

Abstract of Thesis Presented to the Graduate School
of the University of Florida in Partial Fulfillment of the
Requirements for the Degree of Master of Science

DETERMINATION OF RESIDUAL STRESS AND THERMAL BEHAVIOR FOR COMPOSITE LAMINATES

By

William A. Schulz

May 2005

Chair: Peter G. Ifju
Major Department: Mechanical and Aerospace Engineering

As graphite/epoxy composites become more popular in advanced structural design, there is a need to better understand their mechanical behavior in extreme temperature environments. Composites offer many advantages over traditionally used materials; however they tend to be susceptible to residual stress-induced failure. Residual strains, residual stresses, and thermal expansion behavior of IM7-977-2, a graphite/epoxy composite material, are determined over a broad temperature range by using a combination of strain gages and an optical technique called the Cure Reference Method (CRM). CRM is an accurate, full-field, method used to determine the strain on the surface of a composite via Moiré Interferometry. CRM also enables accurate determination of the chemical shrinkage of the epoxy matrix during cure. Classical Laminate Theory (CLT) is widely used to predict mechanical behavior in composite panels, yet it does not account for the chemical shrinkage of the epoxy nor the variation in material properties due to changes in temperature. We developed a method to

characterize multidirectional laminate behavior based on a few tests carried out on a unidirectional laminate. The purpose of this method is to eliminate testing of each desired layup. The transverse modulus E2 has also been measured over a broad temperature range. Other material properties such as fiber modulus, E1, and shear modulus, G12, can also be tested but are not presented in this thesis. By modifying the original CLT formulation to include variations in material properties as a function of temperature as well as chemical shrinkage contributions, one can predict the behavior of a multidirectional laminate based solely on the behavior of a unidirectional sample of the same material system. Testing various layups and comparing analytical to experimental results is used to validate the modifications made to CLT.

CHAPTER 1
INTRODUCTION

Our study focused on characterizing the thermo/mechanical behavior of the IM7/977-2 graphite/epoxy (carbon fiber) composite material system. Carbon fiber composites enable the development of structural materials that are stronger, more durable, and (more important to the space industry) lighter than currently available metal materials. The use of carbon fiber composites has increased exponentially since they were first introduced in the 1960s. They are now implemented in thousands of applications from advanced military weapons and machinery, to automobiles, commercial aircraft, and many household items.

1.1 Reusable Launch Vehicle

Many efforts have been made towards the development of a new space-transportation vehicle. This next-generation vehicle (designed to replace the current STS shuttles and their expendable components) would ideally have a more monolithic design that would be entirely reusable. The vehicle should be completely self-contained and be able to reach orbit, perform its mission, and return all under its own power. NASA's X-33 was the first attempt made at a reusable launch vehicle (RLV). Figure 1-1 shows a conceptual drawing, while Fig. 1-2 shows the construction of the main fuselage.

The X-33 was designed to use a cryogenic fuel source for its propulsion system. Seeing that the desire was to have a completely integrated spacecraft, the fuel tanks shown in Fig. 1-3 were expected to not only carry propellant but act as structural members. For the next-generation RLV to be viable, it is necessary to minimize airframe

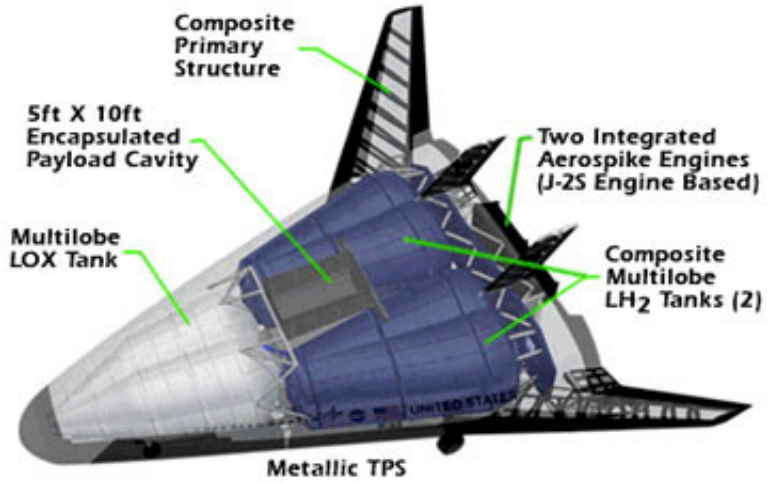

Figure 1-1. Concept design for X-33

Figure 1-2. Fuselage construction of the X-33

weight in order to increase the ability to carry more fuel. By reducing the weight of the fuel tank as well as using it as a structural member, the relative percentage of fuel weight can be increased. To accomplish this goal, advanced composite technology provided the best solution. However, the operating environment of the liquid hydrogen (LH_2) fuel tanks presents a serious challenge for the application of laminated composite materials.

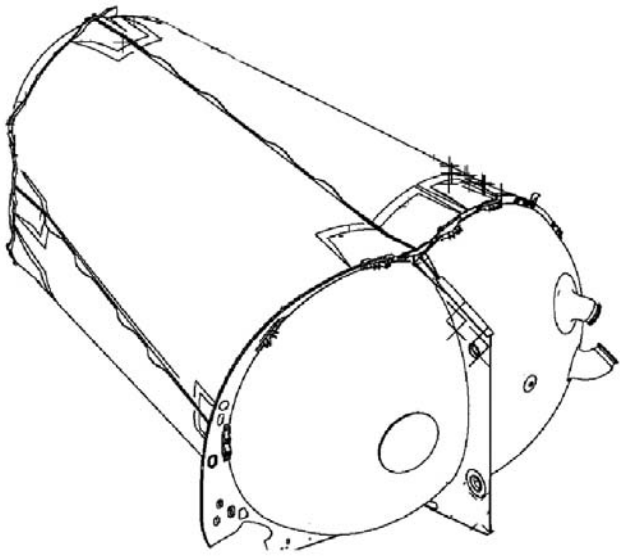

Figure 1-3. Schematic of X-33 LH_2 Fuel Tank

Each fuel tank was designed with a sandwich construction, and several lobes which were bonded together to form the final tank. Each face sheet had a "quasi-isotropic" stacking sequence made of the IM7/977-2 material system and a Korex core. These tanks were designed to support the thermal loads of the cryogenic fuel, and to bear mechanical loads of the aft portion of the RLV. The first tank was constructed and delivered by Lockheed Martin to NASA for testing. Initial testing was done to verify that the tank would be able to withstand the cryogenic temperature loads of LH_2 (-253ºC or 20ºK), as well as the designed mechanical loads. On testing with combined thermal and mechanical loading, the tank suffered a catastrophic failure. A large section of the outer

face sheet of the tank completely delaminated from the core material (Fig. 1-4). In order to safely utilize laminated composites in extreme temperature environments, there is a need to fully understand and quantify the mechanisms that cause thermal stresses within composite materials.

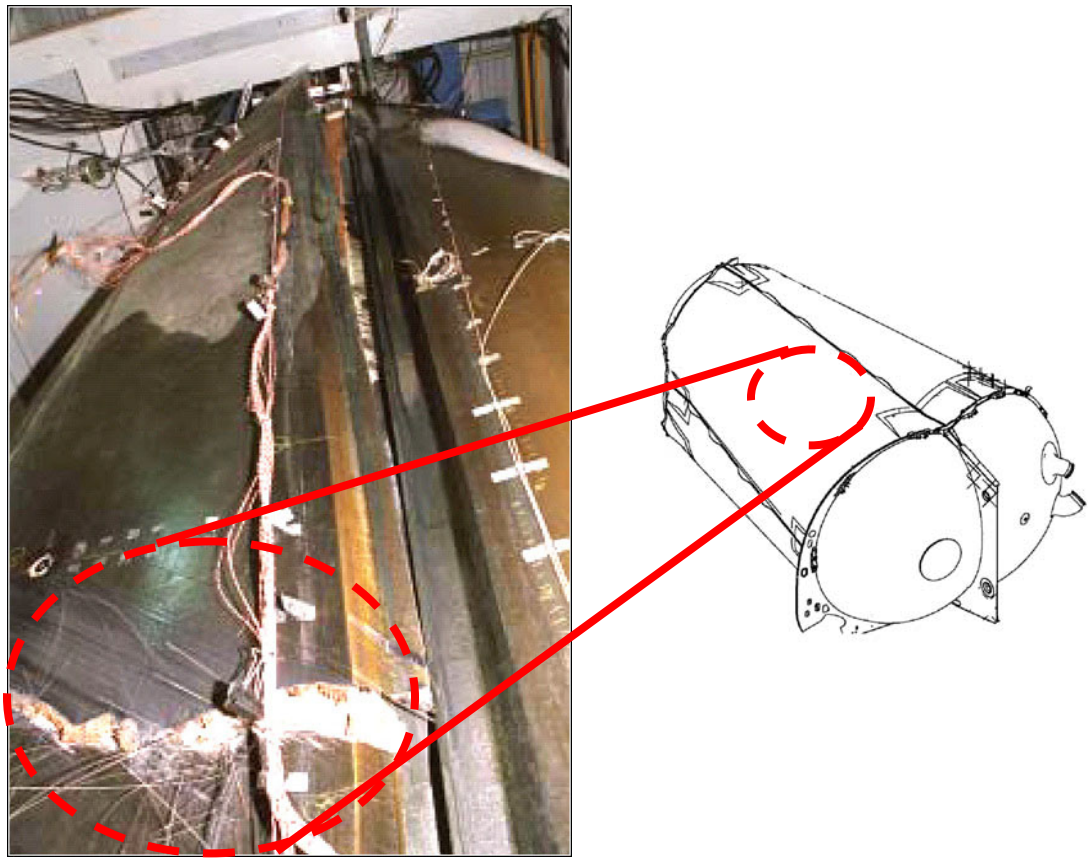

Figure 1-4. Failure of outer face sheet

1.2 Thermal and Chemical Effects

Thermal stresses arise because of the mismatch in coefficient of thermal expansion (CTE) between the fibers and the epoxy matrix in laminates. These stresses can be quite large (up to or exceeding the failure strength of the matrix). In testing of the X-33 LH_2 fuel tanks [1], failure occurred as a result of thermal stress-induced micro-cracks, which led to hydrogen leakage through the face sheet and into the sandwich core. During the

transition back to room temperature, the hydrogen trapped in the core expanded, and catastrophic delamination of the face sheets occurred.

Chemical shrinkage of the epoxy during cure can also induce significant stresses in laminated composites [2, 3]: as much as 15% of the thermal stresses. Chemical shrinkage is a permanent one-time phenomenon that occurs during the initial cure process. The shrinkage is induced by polymerization of the epoxy matrix during the cure cycle. The chemical shrinkage contribution is often neglected in analysis, as it is currently not an easy quantity to obtain. For the same reason, this contribution is rarely considered in experimental work on polymer matrix composites. Neglecting the chemical shrinkage contribution can lead to inaccurate interpretations of the true physical behavior of the composite specimen. At the cure temperature, the composite is commonly assumed to be in a stress free state. Although returning a specimen to its cure temperature will remove the thermal stresses, the chemical shrinkage contribution remains. Through our experiments, it has been shown that the chemical shrinkage of our material system can be significant (as high as 0.2% strain) and consequently should not be neglected.

1.3 Residual Stress

Taken together, thermal stress and chemical shrinkage comprise the residual stress in a composite. On the ply-scale it is possible to minimize the residual stresses by varying the ply angles. For instance, Fig. 1-5 shows that a unidirectional laminate has no residual stresses on the ply-scale, whereas a cross-ply represents the extreme case. The unidirectional ply has a desire to freely expand in the transverse direction as there are no fibers inhibiting the expansion. For the cross-ply however, the desire for one layer to expand is restrained by the desire of its neighboring ply to expand in the opposite direction. A unidirectional composite, free from constraint, is a poor choice for carrying

transverse-to-fiber mechanical loads. Therefore, there is a tradeoff between load carrying strength and thermal strength, the latter referring to the ability for a material to avoid micro-cracking at low temperatures. Trying to obtain the best orientation of plies for a specific task lends itself to a necessity for optimization studies. The experimental results obtained from this research are intended to be used as inputs in optimization studies.

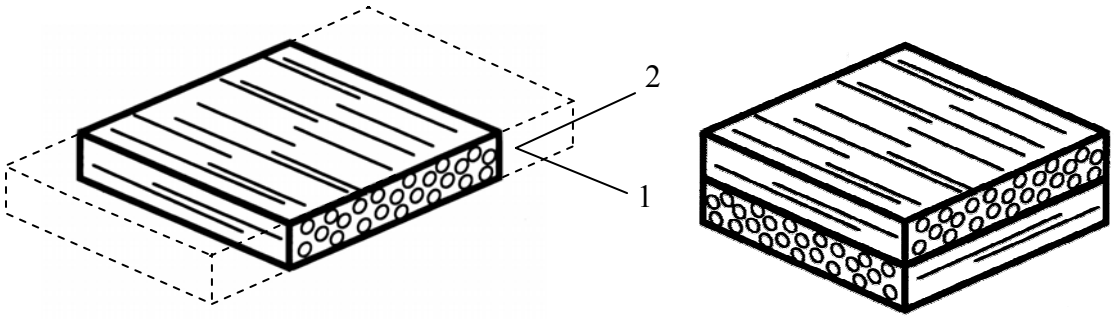

Figure 1-5. Ply interaction: Unconstrained expansion in the transverse direction of a unidirectional ply causes no stresses. Having multiple layers constrains the ability to freely expand, and consequently stresses develop.

Many methods exist that can yield the residual stress in a composite. These methods consist of both computational techniques, usually a form of finite element analysis, and experimental techniques. Many experimental techniques are destructive in nature [4, 5, 6] and once a specimen has been tested it is no longer viable for use or further evaluation, which is highly undesirable. For this reason, many non-destructive techniques have been developed and implemented. These include sensor-embedding [7, 8], X-ray diffraction [9], and the Cure Reference Method [10, 11].

CHAPTER 2
PURPOSE

Due to an increase in the desire to use composites, many methods to predict and characterize the behavior of laminated composites have been created. There are two widely accepted methods that are used to evaluate composite behavior; Finite Element Analysis (FEA) [12] and Classical Lamination Theory (CLT) [13]. The problem that arises is that the benefits of one method can be the faults of the other and vise versa. FEA, if properly applied, can produce accurate results at the expense of large amounts of time. Whereas CLT, in its current form, produces "ball-park" results which can be 20%-25% in error, but is computationally efficient. The dilemma then arises; does one spend hours obtaining an accurate result, or is a general feel for the behavior of the composite, obtained in seconds, sufficient for the purpose. Thus there is a need for a method that can give accurate results in a short amount of time.

2.1 Goals

The goal of this research was to accurately determine the residual stress and thermal properties as functions of temperature, for the IM7/977-2 material system, in a non-destructive manner via CRM and conventional strain gage technology. These thermal properties and behaviors are then to be used to improve optimization studies. Knowledge of this behavior is critical if composite materials are going to be utilized for advanced space transportation technologies. A second goal, yet equally as important, was to improve the predictions generated with Classical Lamination Theory. This analytical technique is used to predict stresses, strains, and curvatures for arbitrarily

stacked laminates, while they endure mechanical, moisture, and thermal loads. The ability to obtain accurate composite behavior would allow these materials to be better understood and more properly applied.

Several samples of each of three prepreg laminates of the IM7/977-2 material system shown in Fig. 2-1 were produced for analysis:

- 13 layer unidirectional layup (UNI) $\left[0_{13}\right]$
- "Quasi-isotropic" layup, from the X-33 (RLV) $\left[+45/90_3/-45/\overline{0}_3\right]_S$
- Optimized angle ply (OAP) $\left[\pm 25\right]_{nS}$

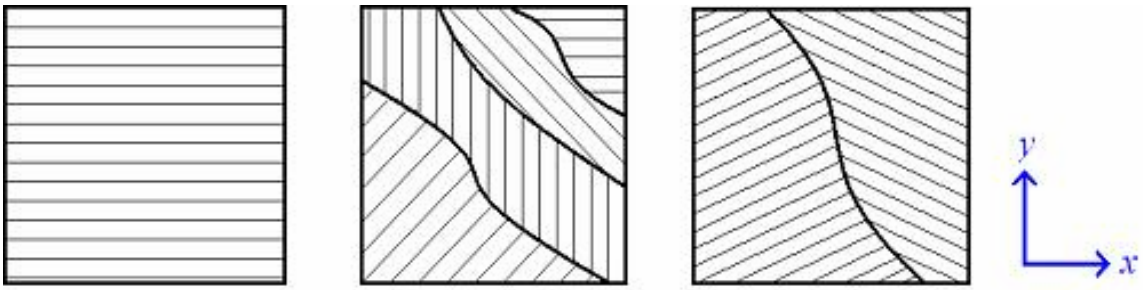

Figure 2-1. Prepreg layups. A) Unidirectional. B) "Quasi-isotropic". C) Optimized angle ply.

The "quasi-isotropic" layup is taken from the design of the LH_2 tank used in the NASA X-33 project. The layup of the optimized angle ply sample stems from a reliability optimization performed by Qu et al. [14, 15], of a LH_2 fuel tank constructed from a graphite-epoxy system. The stacking sequence for the tank was $[\pm\theta_1/\pm\theta_2]s$. Optimal designs had ply angles θ_1 and θ_2 which were near +25° and -25°, and nearly equal; the stacking sequence was thus simplified to $[\pm\theta]s$. It should be noted that this optimized ply sequence was developed for a different material system, but it was used as a starting point to accrue statistical data on typical layups.

2.2 Variability and its Contribution to Reliability

Variability is also an extremely important quantity to obtain. Our current research aims at being able to reduce design weight by reducing the variability in properties input into reliability-based optimization studies. Current deterministic design practices employ safety factors in order to ensure reliability. This method, although effective, results in the addition of extra material and consequently weight. Probabilistic designs, which allow a design to be based on probability of failure, allow you to set target functions, such as minimizing the weight. The previous LH_2 tank optimization study showed that the tank skin thickness was highly affected by the variability in certain input material properties. Figure 2-2 [14] shows the important role of variability in optimization studies. The solid curve represents the initial analysis of the study while the dashed curve represents the same study when the variability in the ultimate transverse tensile strength $\left(\varepsilon_2^{ult}\right)$ was reduced by 10%. What this shows is that a variability reduction of 10% in that single property resulted in a 15% reduction in thickness, and more importantly weight, for the same probability of failure of 10^{-6} (1 in 1,000,000).

2.3 Analytical Prediction

Classical Lamination Theory is a widely used analytical method to predict laminate behavior. However, it will be shown that important material behaviors are not accounted for in its current form. The relative error between prediction and experimental results can be as high as 25%. This is a large discrepancy, which would need drastic reduction in order for someone to gain confidence in the values produced by the model. Understanding the sources of these discrepancies is a crucial step towards making a better prediction. The main sources being that the model does not account for the volumetric

shrinkage of the epoxy resin as it cures or the thermal variation of material properties due to changes in temperature. The theory was modified to account for these current discrepancies in the model and will be discussed in detail in Chapter 6.

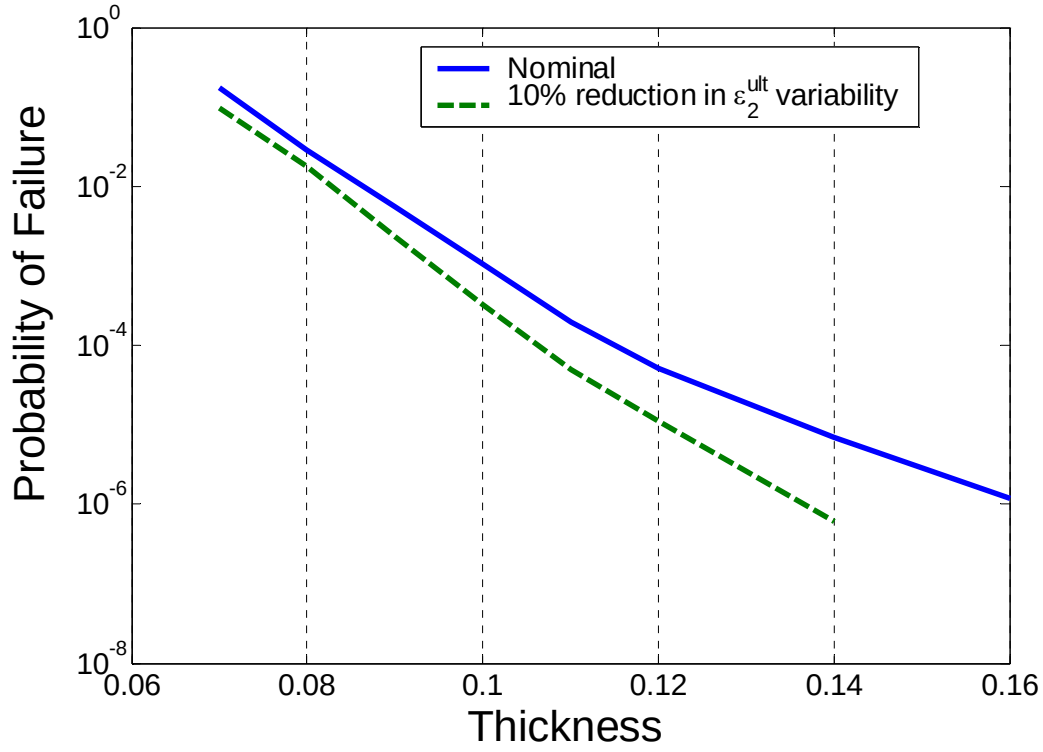

Figure 2-2. Effect of variability on tank skin thickness

CHAPTER 3
CURE REFERENCE METHOD

3.1 Background and Significance

Residual and thermal stresses can be determined by using the Cure Reference Method to measure the residual strain in unidirectional or multidirectional composite laminates. CRM uses the full-field laser based optical method of Moiré Interferometry to document strains on the surface of laminates that initiate during the high temperature curing process. The method involves the replication of a high frequency diffraction grating on a specimen while in an autoclave. The grating acts as a reference to the stress free condition just prior to resin solidification, at the cure temperature of the epoxy. Since the grating is cured with the composite, it carries the same thermal strain and chemical shrinkage information as the composite. Subsequent strains result from two mechanisms, the chemical shrinkage of the polymer matrix and the thermal mismatch between the resin and matrix.

3.2 Moiré Interferometry

The heart of the Cure Reference Method is the technique of Moiré Interferometry. Moiré Interferometry is a laser based optical technique that can be used to determine a contour map of in-plane displacements. Moiré is characterized by high displacement and strain sensitivity, high spatial resolution, and a high signal to noise ratio [16]. It is a non-contacting, full-field method capable of measuring both normal and shear strain. A schematic of the Moiré Interferometry setup can be seen in Fig. 3-1. The actual interferometer, with a specimen, can be seen in Fig. 3-2. The technique is based on the

principal of the constructive and destructive interference of light. The result of the interference is a very characteristic pattern of light and dark fringes as seen in Fig. 3-3. These fringe patterns can be used to directly determine the in-plane displacements. Knowing the in-plane displacements leads to calculation of in-plane strains and residual strains, which then lead to determination of residual stresses in each ply.

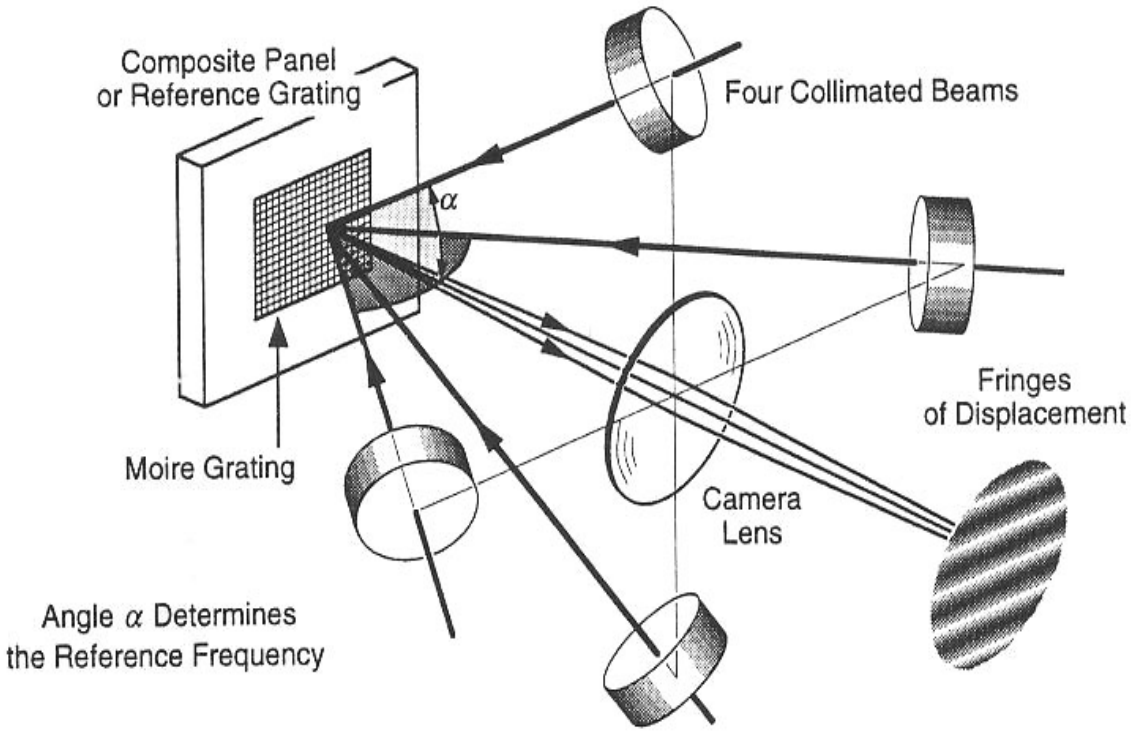

Figure 3-1. Four-beam Moiré Interferometer schematic

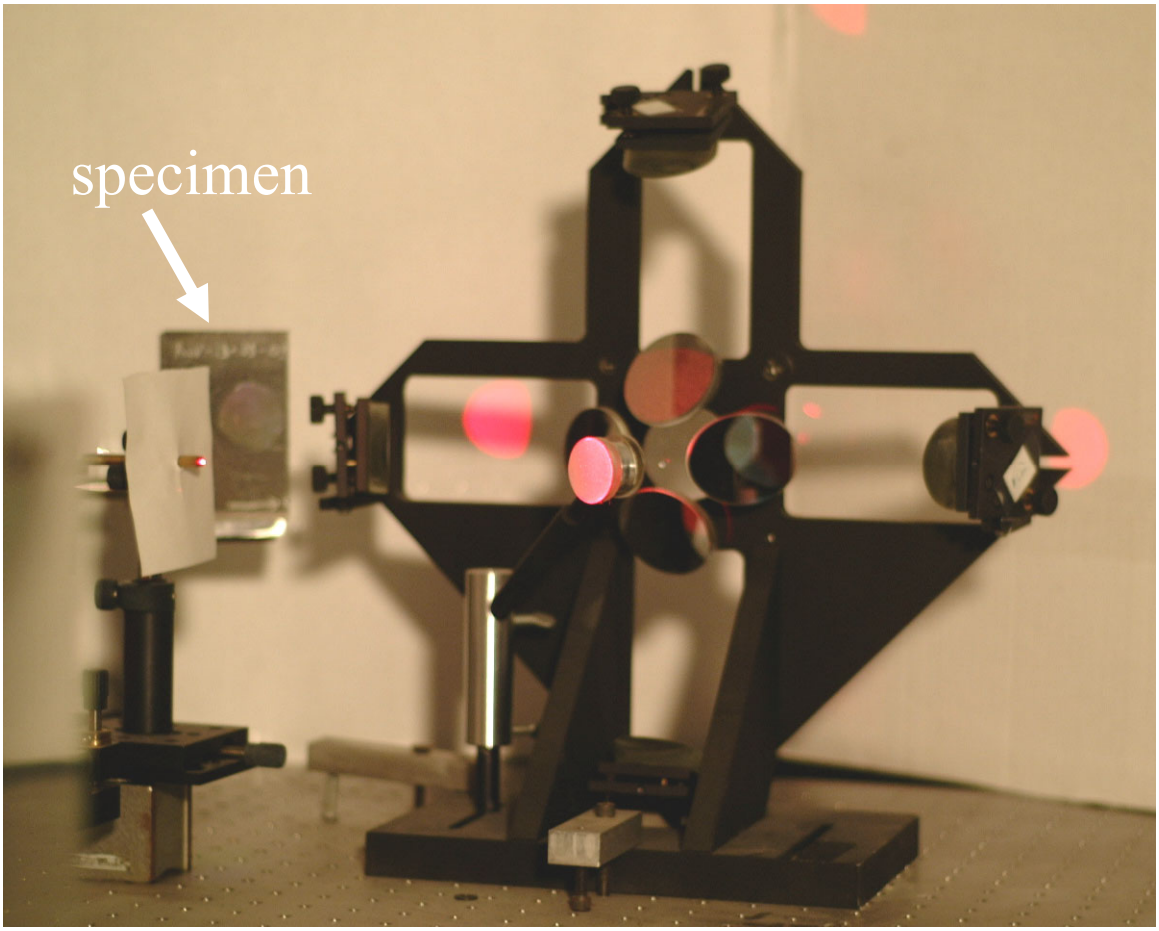

Figure 3-2. Four-beam Moiré Interferometer

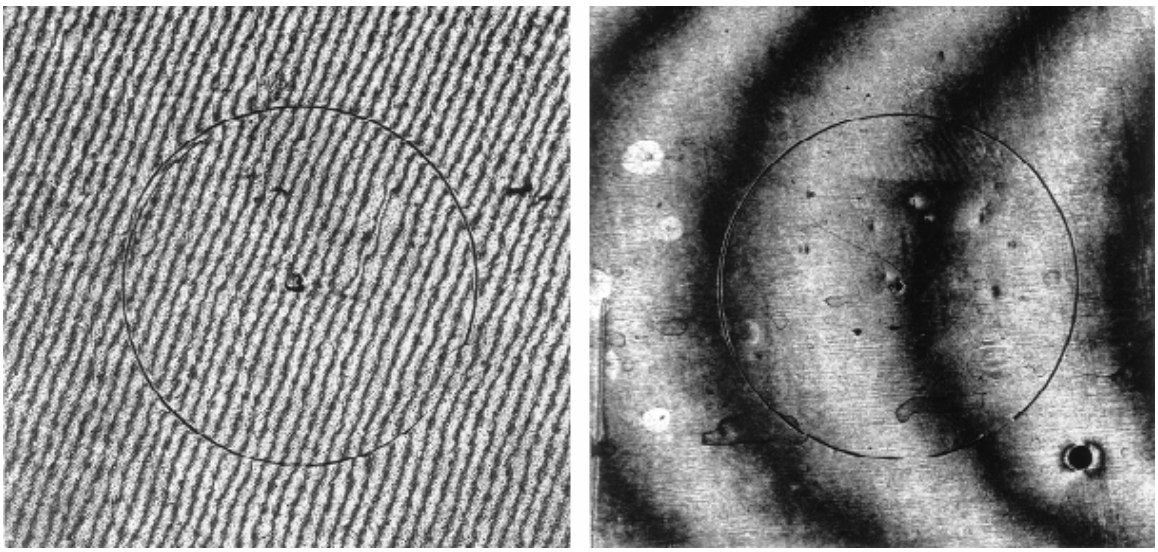

Figure 3-3. Typical fringe patterns (scribed circle is 1-inch diameter)

3.3 Grating Production

The process by which a diffraction grating is produced for application to a composite laminate involves several steps which are outlined in detail in references [2, 11]. The final stage is the production of the autoclave tool that consists of an aluminized grating on a 5” x 5” x ½” piece of astrosital Fig. 3-4. Astrosital is an ultra low expansion (ULE) glass with a coefficient of thermal expansion (CTE) of $0.3x10^{-7}$ mm/mm/°C. The low expansion of the tool is necessary so that the tool does not transfer any thermally induced strain to the grating on the panel during the transfer process in the autoclave.

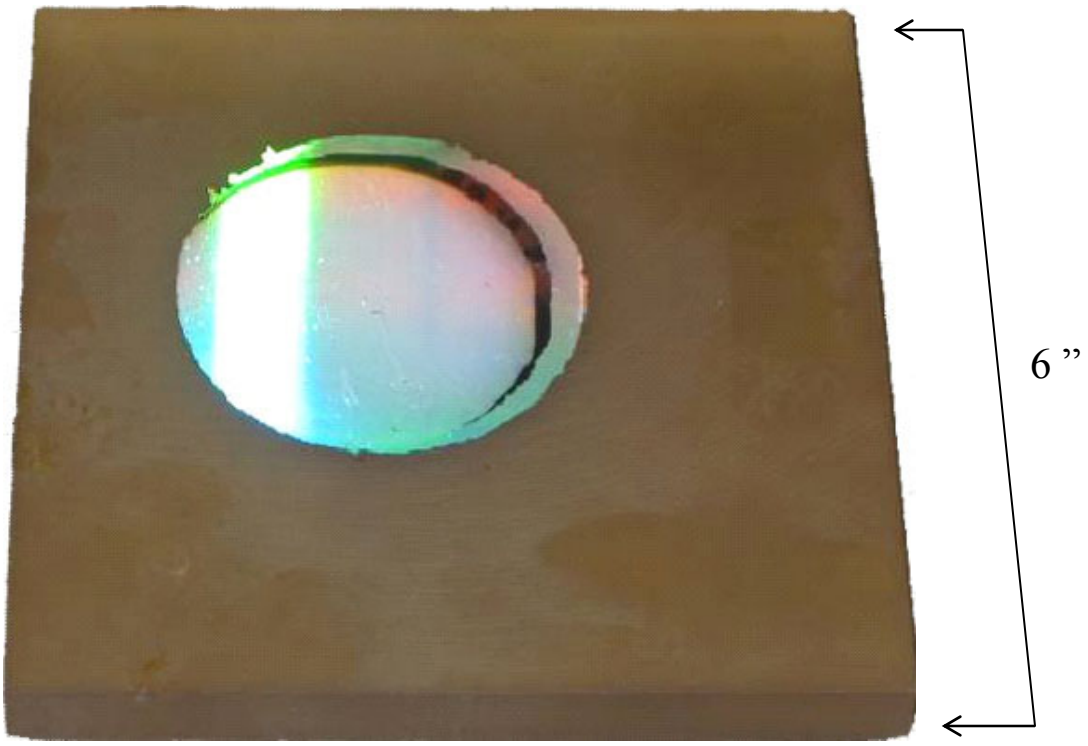

Figure 3-4. Astrosital autoclave tool with attached grating

3.4 Autoclaving and Grating Transfer

Most high performance composite laminates are produced with the use of an autoclave. The autoclave is a pressure oven that has vacuum line connections within the pressurized chamber. Once the stacking sequence for the specific laminate is chosen, one

can process the laminate and apply the diffraction grating by following the steps listed below.

1. **Layup:** Assemble the laminate in the specific stacking sequence that has been prescribed.

2. **Vacuum bagging:** Figure 3-5 shows a schematic of the vacuum bag assembly. The ULE Astrosital tool with the grating side up is placed at the base of the assembly and the surface is then covered with a nonporous release film. A hole of approximately 1.5" diameter is cut into the release film, which allows for the grating to be exposed to the composite surface during the cure cycle. It is critical that the film thickness is as minimal as possible so that it will not interfere with the transfer of the grating to the composite during the cure process as the resin begins to polymerize. The prepreg laminate is then placed on top of the release film, centered over the ULE tool, and appropriately aligned with the grating. The non-porous release film placed between the tool and the laminate prevents the epoxy from curing to the tool. A layer of porous release film is placed on the upper surface of the laminate, which provides two functions, allowing excess resin to be drawn off the laminate and into the bleeder cloth, as well as for separation from the bleeder cloth. The bleeder cloth is a porous material that absorbs excess resin drawn out of the laminate via vacuum, which allows an appropriate fiber volume fraction to be achieved. The breather cloth, which can be the same material as the bleeder cloth, is used to distribute the vacuum throughout the entire bag. Another layer of non-porous release film is placed between the bleeder and the breather cloths so that excess resin is not transferred into the breather material resulting in resin being drawn into the vacuum line or clogging the breather cloth which would prevent an even vacuum distribution on the laminate during cure. Finally the ULE and laminate assembly are placed into a vacuum bag; sealed with a sealant tape, and placed in the autoclave for curing.

3. **Cure preparation:** The vacuum bag is connected to the vacuum line. Vacuum is applied and a leak check is performed. It is imperative that the vacuum integrity is maintained, throughout the necessary portions of the curing process, as a poor vacuum can lead to a resin rich laminate.

4. **Cure:** Execute the appropriate cure cycle (Fig 3-6) for the epoxy matrix material.

5. **Grating transfer:** Once the composite has reached the cure temperature the autoclave is opened and the panel is separated from the ULE tool as quickly as possible. Upon separation, the diffraction grating is transferred to the composite panel. The panel is then placed back in the autoclave to finish the remainder of the curing process.

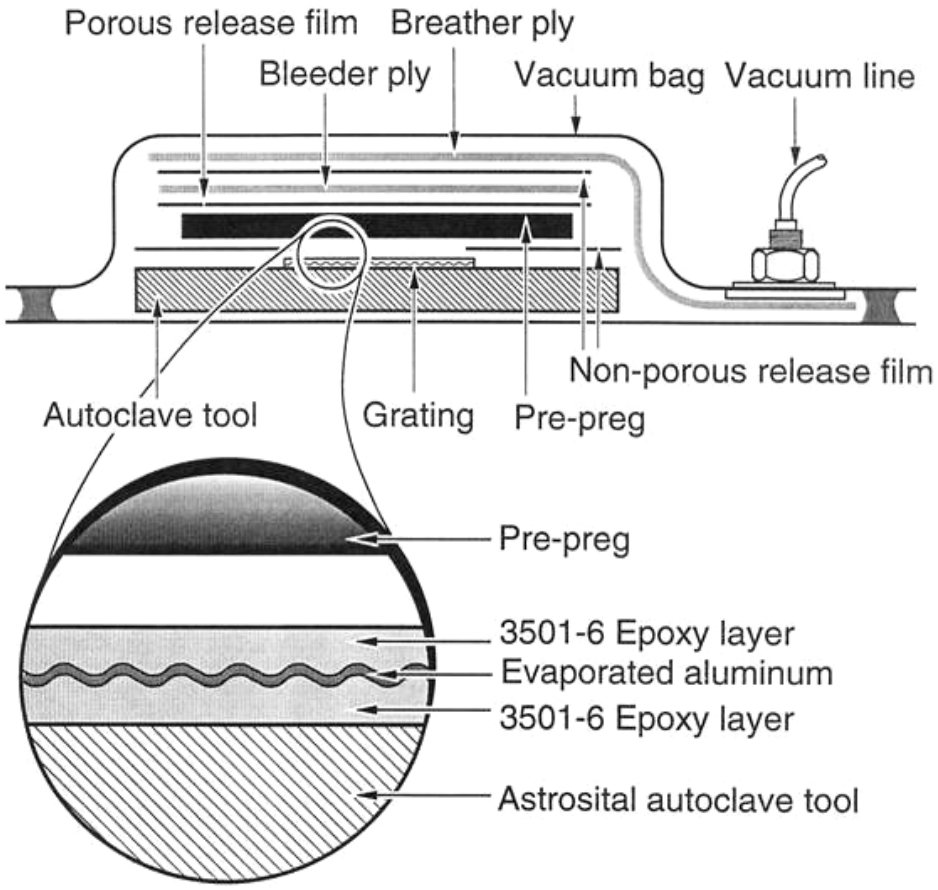

Figure 3-5. Vacuum bag schematic

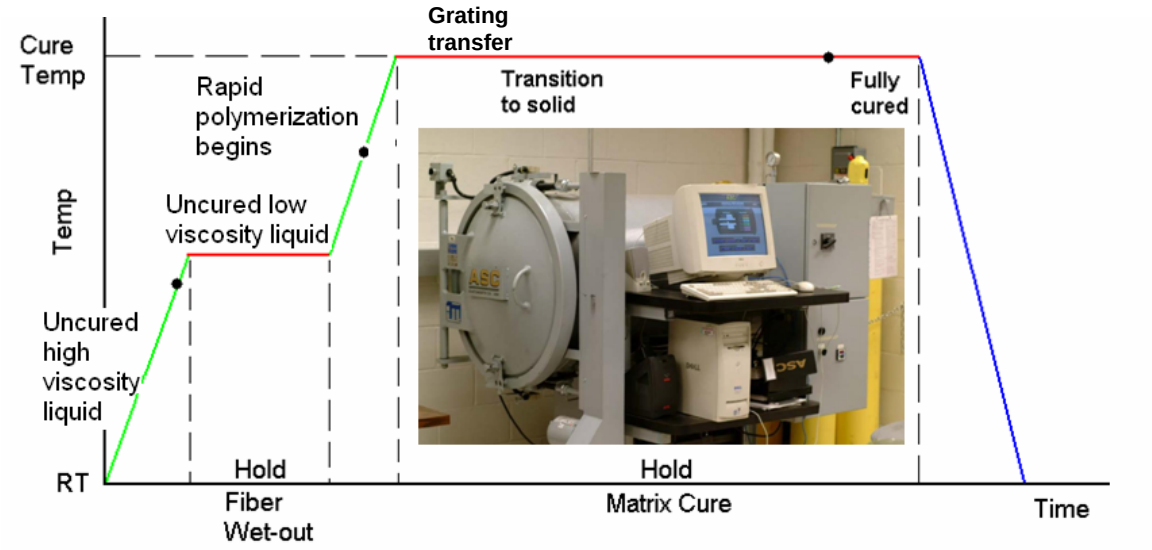

Figure 3-6. Autoclave and representation of cure cycle

After the composite panel has finished the cure cycle, the specimen is then ready to be analyzed. The grating, which was applied at the cure temperature, bonds to the specimen and consequently records any deformation that the panel experiences as it cures. This deformation can then be analyzed with Moiré Interferometry which is discussed in the next section. A panel with a transferred grating can be seen in Fig. 3-7.

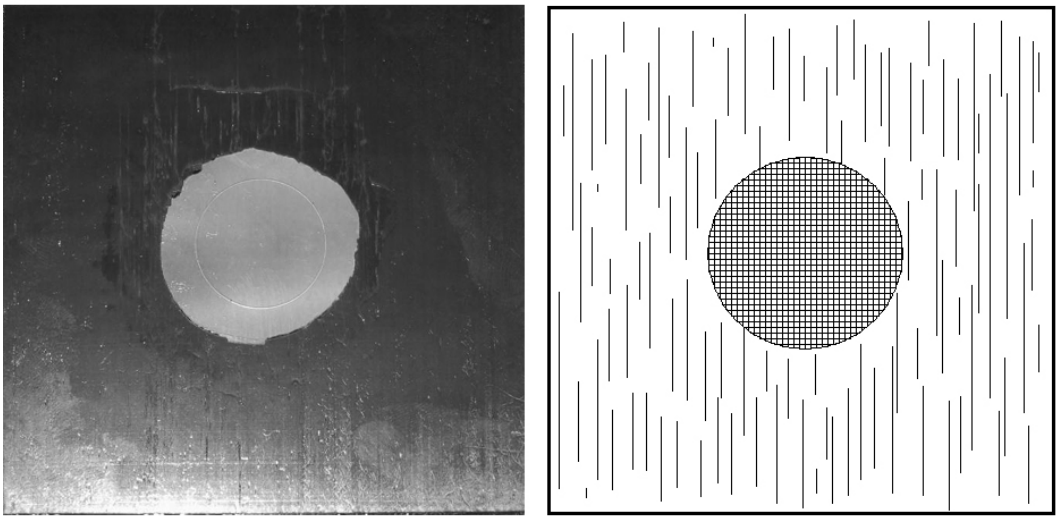

Figure 3-7. Cured composite specimen and schematic with attached grating

3.5 Data Analysis

Once the fringe patterns on the specimens have been photographed, the resulting displacement field images need to be analyzed. As seen in Fig. 3-3, the resulting images are a pattern of light and dark bands, where each dark band is referred to as a fringe. The fringe order, or number of fringes (N), is directly related to the displacement of the composite panel. For this particular application, the displacement sensitivity is 0.417 microns per fringe order, which means that a specimen has been displaced 0.417 microns between two consecutive fringes. The relationship between the fringe order and the displacement are shown in Eqs. (3-1) and (3-2) for the horizontal (U) and vertical (V) displacement fields respectively.

$$U = \frac{N_x}{f} \tag{3-1}$$

$$V = \frac{N_y}{f} \tag{3-2}$$

Where *f* is the frequency of the virtual reference grating that is created inside the interferometer, in this case the frequency is 2400 lines/mm, and N_x and N_y are the number of fringes in the vertical and horizontal images. Now that a relationship between displacements and the number of fringes has been established, the absolute strains can then be determined by taking the derivative of the displacements as shown in Eqs. (3-3) and (3-4).

$$\varepsilon_x = \frac{\partial U}{\partial x} = \frac{1}{f}\left[\frac{\partial N_x}{\partial x}\right] = \frac{1}{f}\left[\frac{\Delta N_x}{\Delta x}\right] \tag{3-3}$$

$$\varepsilon_y = \frac{\partial V}{\partial y} = \frac{1}{f}\left[\frac{\partial N_y}{\partial y}\right] = \frac{1}{f}\left[\frac{\Delta N_y}{\Delta y}\right] \tag{3-4}$$

Where ΔN_x and ΔN_y represent the number of fringes that are seen over a given gage length of Δx or Δy on the respective image.

With these measurements, a room temperature reference point of the true surface strain on each panel is able to be attained. This room temperature measurement is the keystone to obtaining an accurate relationship of the strain and thermal expansion, or contraction, as a function of temperature for the composite specimens. This data point will allow strain gage measurements, discussed in Chapter 4, to be superimposed so that an accurate representation of the surface strain can be established. Results from the CRM experiments are discussed in Chapter 5.

3.6 Error Sources

Errors can be introduced in several ways while implementing CRM. All sources of error must be considered, in order to produce accurate and reliable results from this technique. Although not necessarily a significant source of error in these experiments, error can be introduced by a misalignment of the diffraction grating. If a grating is not properly aligned with the desired measurement direction, it will yield inaccurate results. For instance, a two degree misalignment of a grating would result in measuring the strain in the 2° and 92° directions, as opposed to the desired 0° and 90° directions. The data obtained would be that of a rotation in the strain measurement and results are shown in Fig. 3-8. It can be seen that for most cases a 2° misalignment can introduce small errors in measured results.

The layup of the panel can also introduce errors into measured results. All plies are assumed to be aligned in the specific direction designated in the stacking sequence. However, since the panels were laid up by hand there exists a chance that the fibers were not aligned perfectly with the desired direction. If a single ply or a number of plies were misaligned, they will cause the panel to behave differently and consequently affect measured results.

Other errors can be introduced via the interferometer. Every precaution should be taken to assure that the interferometer is properly tuned, and that the specimen is in the correct orientation and position. Due to the high sensitivity of this technique, minor vibrations can also affect the images taken of the displacement fields.

Although there are many ways errors can be introduced with this technique, they were all accounted for during testing, to the best of ability, assuring that accurate results were obtained from this technique.

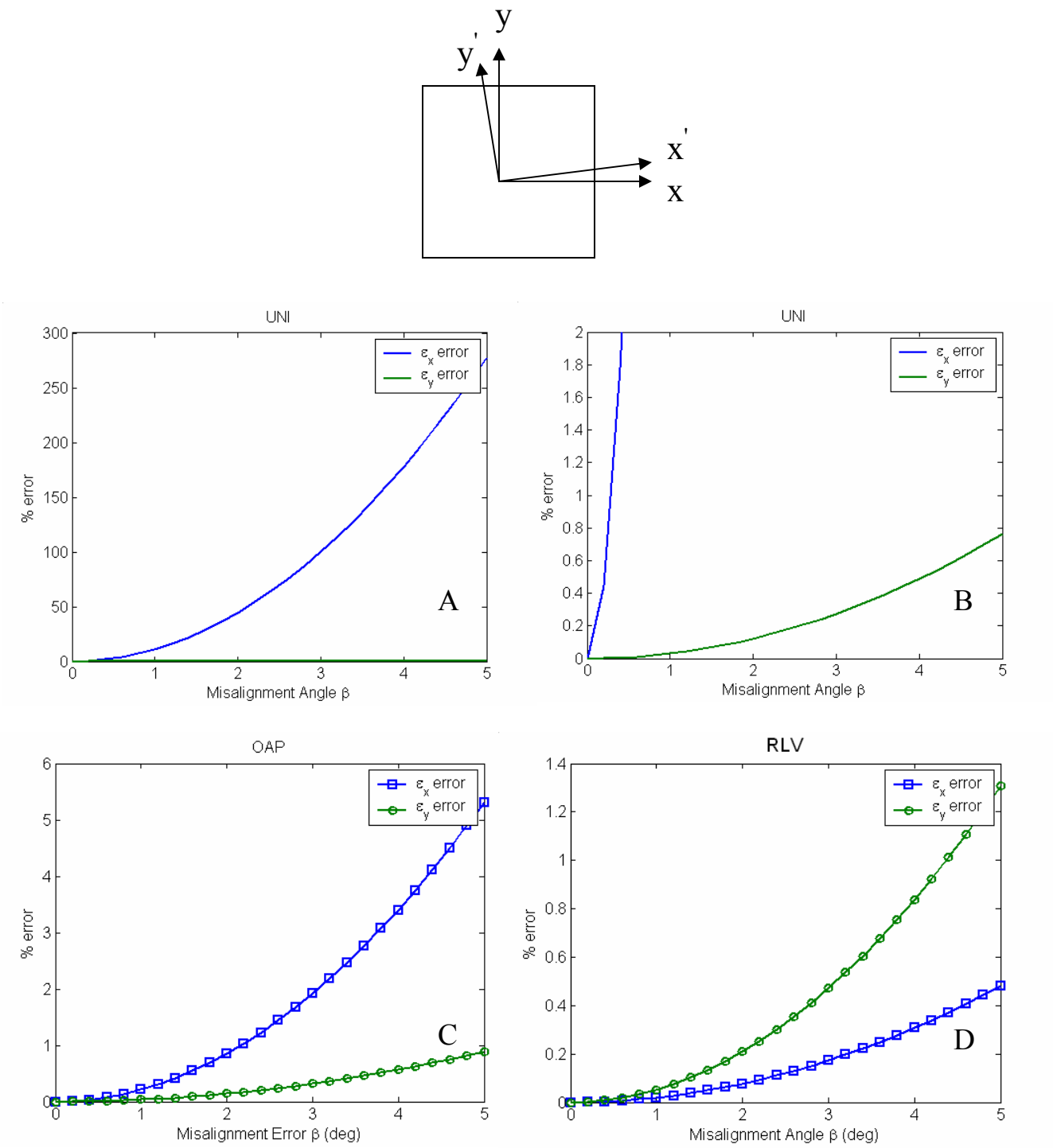

Figure 3-8. Grating misalignment measured strain in % error. A) a unidirectional specimen. B) vertical zoom in of (A) to show more clearly the difference between errors. C) a ±25° OAP specimen. D) a "quasi-isotropic" RLV specimen.

CHAPTER 4
TEMPERATURE VARIATION EXPERIMENTS

The Cure Reference Method which was described in the previous chapter allowed the calculation of a strain reference point on the composite specimens at room temperature. In order to obtain thermal expansion, chemical shrinkage, and mechanical properties, conventional strain gages were used. Strain gages allowed the relative change in surface strain on the specimens to be obtained over a broad temperature range. The foundation of the thermal property testing is discussed in a technical note provided by the gage manufacturer [17].

4.1 Strain Gages

Strain gages are a widely used method to accurately determine the strain on a specimen they are bonded to. Metal foil gages are the most common type of gage used to measure strain on an object. These types of gages are composed of an extremely thin layer of a metallic material, on the order of 0.001 in, bonded to an electrically neutral substrate. The gage is then bonded to a specimen, which is then subjected to prescribed test conditions. The foil of the gages acts as a variable resistor in an electric circuit as shown in Fig. 4-1. While a specimen experiences thermal or mechanical loads, the gage will also experience them, which consequently produces a resistance change in the gage. The change in resistance can be obtained by monitoring the change in applied voltage across the gage as it undergoes loading. This resistance change can then be directly related to strain.

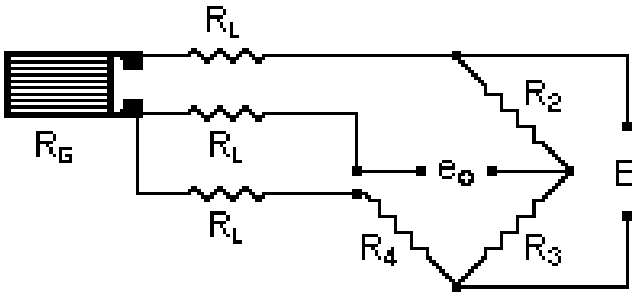

Figure 4-1. Strain gage circuit

4.1.1 Special Considerations

When using a strain gage, it is important to realize their limitations. Failure to do so can produce flawed experimental data which is not representative of the true behavior of the test article. Since foil gages are made of metal, the gages are prone to expand and contract on their own due to temperature changes. When one measures the strain output of a gage, it is comprised of two components. The first being the resistance change in the foil due to thermo-mechanical loads on the specimen, which is the true physical strain on the specimen. The second component is the resistance change due to the thermal expansion or contraction of the gage itself as in Eq. (4-1). At certain temperature ranges, usually around room temperature in most gages, the contribution of this second component is negligible and is often disregarded. However, at temperature extremes this component can constitute as much as 10%-15% of the apparent measured strain. Not taking this "false" strain into consideration will lead to serious errors in measured data. This thermally induced strain is discussed further in Section 4.4.2 and the effect is shown in Fig. 4-10.

$$\varepsilon_{\text{apparent}} = \varepsilon_{\text{thermo-mechanical}} + \varepsilon_{\text{gage foil expansion}} \tag{4-1}$$

In order to obtain the true strain on the specimen, one must remove the strain contribution from the expansion of the gage. Several techniques are in existence which

enables compensation for temperature influences on strain gage readings [18, 19]. A form of dummy compensation was used for testing in this research, and was accomplished by placing a duplicate gage on a material with which the thermal expansion properties are known as a function of temperature. No one material was able to be obtained for the desired temperature range of interest. Therefore, two materials were chosen as references; 1) Ti6-4Al-4V, a titanium alloy, used for measurements below room temperature and 2) astrosital, which is the same material used in the grating transfer process, for measurements above room temperature. The reference material and specimens were placed in the thermal chamber so that they would experience the same thermal conditions. At any given temperature the strain on the reference material can be measured, which is a combination of the thermal expansion of the material and the thermal expansion of the gage itself, exactly as seen previously in Eq. (4-1). However, the expansion properties of the reference material are known as a function of temperature, accurate to 1.5% [20]. The theoretical expansion, of the reference material, due to the temperature change can then be removed from the measured strain Eq. (4-2), yielding the strain contribution due purely to the expansion of the gage itself.

$$\varepsilon_{\text{gage foil expansion}} = \varepsilon_{\text{measured on reference}} - \varepsilon_{\text{theoretical}} \tag{4-2}$$

Removing Eq. (4-2) from Eq. (4-1) yields the true themo-mechanical strain present on the specimen

$$\varepsilon_{\text{true}} = \varepsilon_{\text{apparent}} - \varepsilon_{\text{gage foil expansion}} = \varepsilon_{\text{thermo-mechanical}} + \varepsilon_{\text{gage foil expansion}} - \varepsilon_{\text{gage foil expansion}} \tag{4-3}$$

4.1.2 Gage Selection

Gage selection is extremely important when designing an experiment where strain gages are to be used. There are many different types of gages and each has their specific

application. Typical gages are not rated to handle the large temperature ranges which were of interest to this study. Therefore, custom unidirectional gages, of designation WK-13-250BG-350, that could perform over our desired temperature range, nominally ± 200ºC, were obtained through the Vishay Micromeasurements Group.

4.1.3 Adhesive

In addition to gage selection, the method with which the gage is adhered to the test article must also be considered. For large temperature ranges it was recommended that the M-Bond 610 epoxy adhesive system, also from Vishay, be used to attach the gages to the specimens.

4.2 Specimen Preparation and Gage Application

Specimens for both the thermal expansion and transverse modulus measurements were prepared in similar fashions according to NASA recommended strain gage application procedures [21] which are briefly listed below.

- Each specimen was abraded, with varying grits of sand paper, to remove any surface flaws, and to provide a uniform surface for good gage adhesion. The specimen surfaces were also chemically conditioned with an acidic solution during and after the abrasion process to aid in the abrasion process. The surfaces were then neutralized and wiped clean of any residue.
- Perpendicular gage marks were applied to test specimens for gage alignment
- Gage and strain relief tabs were aligned on specimen and attached to a strip of Teflon tape.
- The tape was peeled back exposing the underside of the gage and strain relief tab. The gage, relief tab and surface of the specimen was then coated with a thin layer of M-Bond 610 adhesive, which was then allowed to air dry for 10 minutes.
- After drying the gage was placed back on the composite specimen and clamped with uniform pressure through silicon rubber tabs placed on top of the gage.
- As recommended the specimen was then placed in an oven and the temperature was raised to 121°C and remained there for three hours. After the initial cure the clamps were removed and the specimens were placed back in the oven for a post cure at 135°C for two hours.

4.2.1 Coefficient of Thermal Expansion Specimens

The same specimens that were used for the Cure Reference Method experiments were used to determine the surface strain and the coefficient of thermal expansion data. Using the same specimens allowed for a direct correlation between the initial strain reference point obtained via CRM and the strains measured due to temperature variation. The panels were sectioned so that 1) the original grating could be maintained so that if needed, it could be reanalyzed at a later time and 2) there was enough material to allow accurate strain readings without edge effect problems. The panels were nominally 4"x 4" in dimension when produced. Approximately 1/3 of the panel or 1.5 inches was cut from the original specimen with a diamond cutting saw. Each specimen had a total of four gages attached to its surface. A gage in the x and y directions was applied to both sides. The *x* and *y* gages were then averaged during the experiment to obtain an average strain value through the thickness. A schematic can been seen in Fig. 4-2.

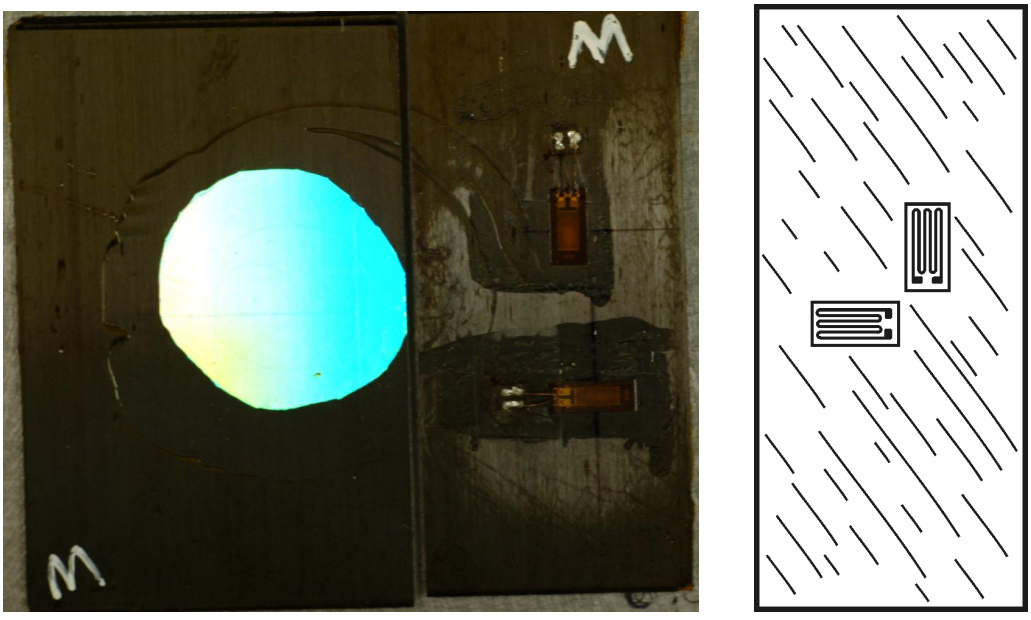

Figure 4-2. Composite panel and schematic with attached gages

4.2.2 Transverse Modulus Specimens

Transverse modulus specimen geometry was prepared according to ASTM standard 3039 [22]. The only deviation from the standard was that the specimens were made to be 12” in length in order to accommodate the gripping fixtures. An 18 layer, nominally 0.090” in thickness, unidirectional 12” by 12” panel of IM7/977-2 was produced in the autoclave. Four strips of G-10 fiberglass, of dimension 1/16” x 1.6” x 12”, were bonded with Hysol 9394 to the panel for tabs. The panel was then cut into 1.25” wide coupons with a diamond cutting wheel. These coupons were then placed in a surface grinder and both edges were ground to remove edge flaws that were produced during the initial cutting. Edge flaws can promote crack propagation within the specimen, which can lead to premature failure during testing. Each test coupon, seen in Fig. 4-3, were ground till the width nominally reached 1.000”.

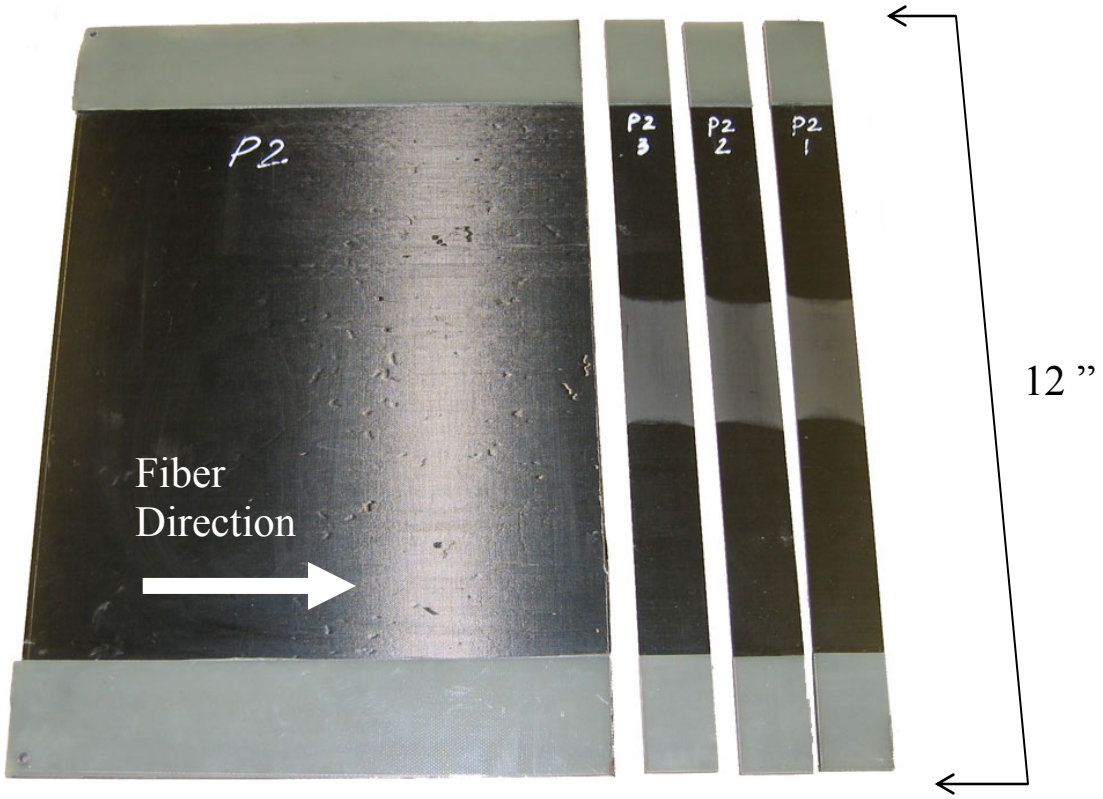

Figure 4-3. Transverse modulus panel with cut specimens

4.3 Experimental Setup and Application

This section describes the equipment used to perform the temperature variation experiments. A liquid nitrogen (LN_2) dewar was attached to a Sun Systems Model EC12 environmental chamber which is seen in Fig. 4-4. The chamber is able to regulate the temperature about a desired point by controlling heating elements and the release of LN_2.

Figure 4-4. Thermal chamber and LN2 dewar

4.3.1 Coefficient of Thermal Expansion

Three specimens were tested in the environmental chamber during an individual experiment. The specimens and the reference material were placed inside the chamber on a sheet of Teflon (Fig. 4-5). The Teflon minimized the friction between the specimens and the oven structure so they could experience free thermal expansion. The oven was first set to 24°C so the gages could be zeroed out at the same temperature that the CRM results were obtained. After the gages had been zeroed out at room temperature, the temperature was varied from approximately -200°C to 200°C, and data was acquired at

20 degree intervals. For accurate results, thermal equilibrium must be achieved at each set temperature point. The specimens were held at a given temperature for 25 minutes, which allowed the temperature to stabilize within the chamber and maintain a constant value for a minimum of 20 minutes as per ASTM standards. After the holding period, the strain on the panels was acquired and stored in a data file for further use.

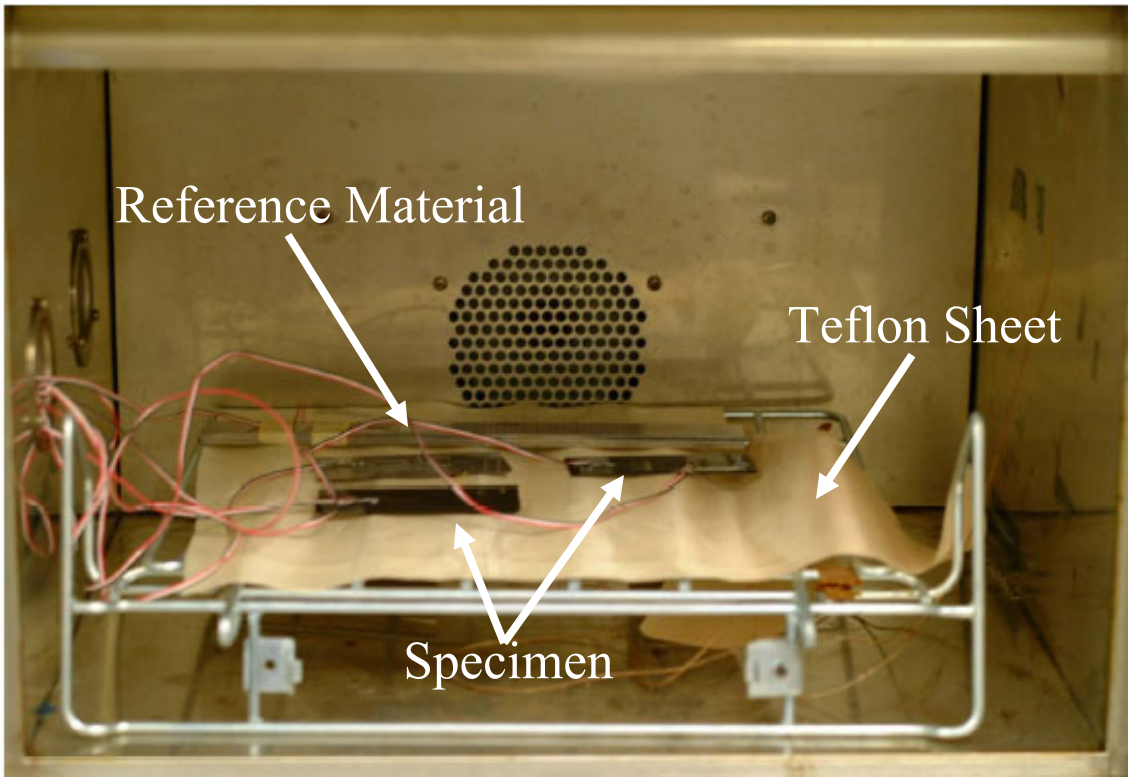

Figure 4-5. CTE specimens inside thermal chamber

The lead-wires from the specimen gages were passed through a removable port and attached to the bridge completion device. Each gage was read in a quarter-bridge configuration where the lead wires were passed into a STB-AD808FB Optim Electronics 350 Ω quarter-bridge completion module. The completed bridges were then read by National Instruments data acquisition hardware. A SCXI-1322 breakout board attached to a NI SCXI-1122 sixteen-channel isolated transducer multiplexer module was used for

the CTE measurements, as each experiment had a total of 13 gages; 3 specimens with 4 gages each and one gage on the reference material.

It is important to note that the strain that was measured was only the relative change in strain from the zero strain reference state, 24°C, to the specific temperature where the measurement was being taken. The composite panel had a preexisting state of strain at room temperature which was measured with CRM and was included after the relative changes in strain were measured.

4.3.2 Transverse Modulus

After the specimens were cut from the panel and the gages were applied, the specimen was then placed in the specially designed grips. The grips were designed around several specifications:

- Existing grips are bulky and present a large thermal mass. Therefore grips had to be designed with a lower thermal mass and thus less bulky.
- They must be easy to operate and attach to current loading machine.
- Grips must be heat treated to strengthen and prevent failure.

The specimen was attached to the grips through the use of an alignment fixture, Figures 4-6 and 4-7, which was machined out of a dense, yet easily machinable, foam. This fixture forced the specimen to be aligned between both grip ends. Having nearly perfect alignment of the specimen within the grips assured that there would be no load misalignment during testing. Loading misalignment can produce specimen bending, and introduce errors into the experimental data read by the strain gages. Misalignment can also cause premature failure of the specimen, which renders it useless for further testing.

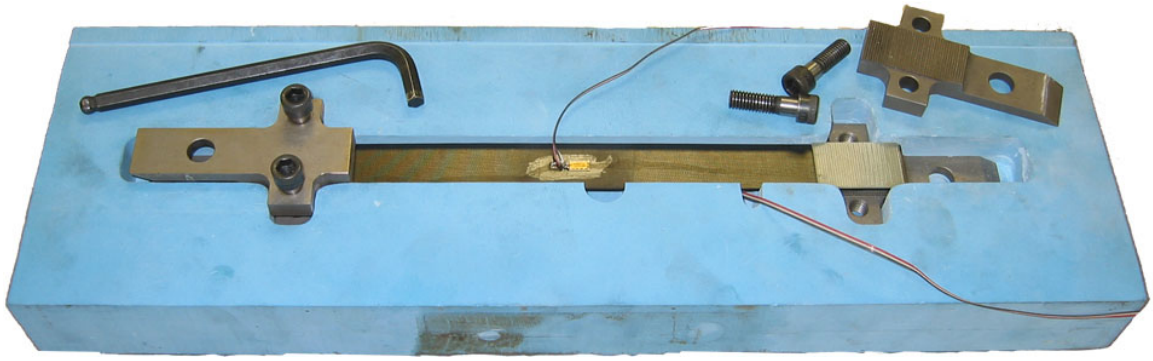

Figure 4-6. Specimen alignment fixture with specimen and grips

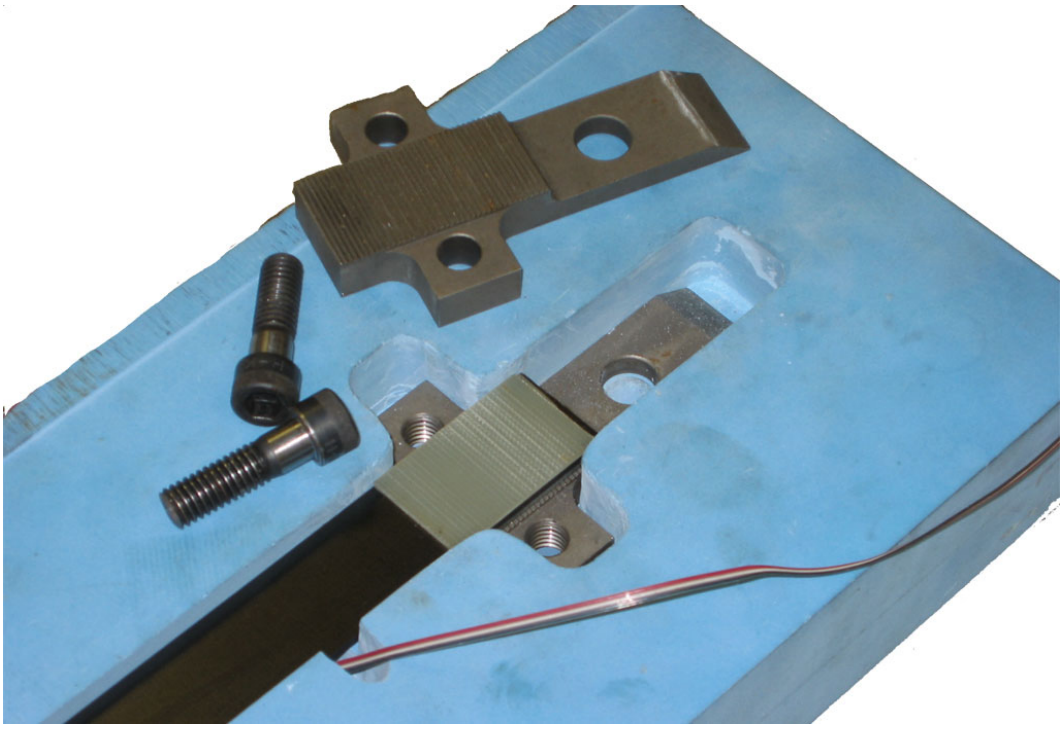

Figure 4-7. Gripping fixture and specimen in alignment tool

After the specimen was placed inside the grips, the entire assembly was loaded into a standard screw driven tension/compression machine. Once the specimen was placed in the testing machine, a thermal chamber made of Rohacell 110-IG foam was placed around the specimen and grips, as seen in Fig. 4-8, which was then sealed with tension straps. Rohacell was chosen as the chamber material because of its ability to resist deformation at high temperatures, machineability, and its thermal insulation properties.

A NI SCXI-1121 four channel module was used for the modulus testing, and was used to read gages, control loading, and read the diode temperature sensor. Each specimen was tested at 14 points, at approximately 25°C intervals, from -165°C to 150°C. The specimen was allowed to soak for 20 minutes, as per ASTM standards, at each new temperature to allow the specimen to reach an equilibrium temperature.

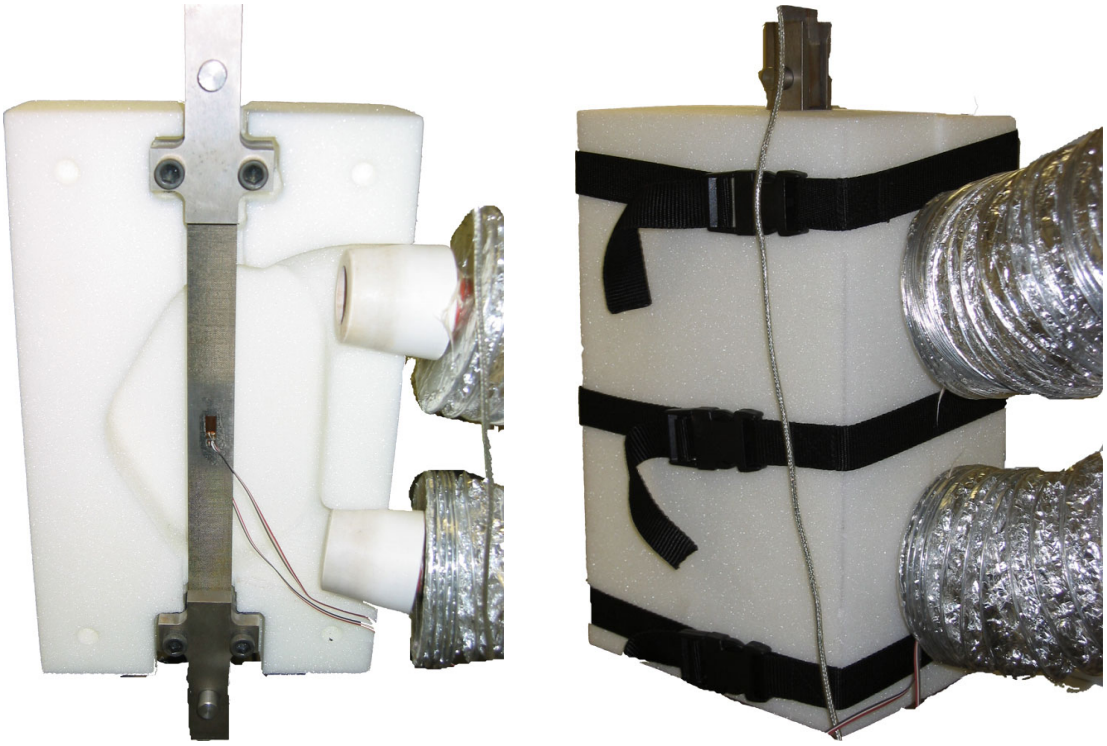

Figure 4-8. Rohacell thermal chamber with specimen, open(left) and closed(right)

4.4 Error Sources

If improperly used, strain gages can produce significant errors. In most cases, a strain gage will display some strain value. It is up to the user to determine whether the results are feasible and more importantly, accurate.

4.4.1 Gage Alignment

For most composite applications, or any non-isotropic material, strain gages become highly sensitive to misalignment [23]. Significant time and detail was spent on

strain gage alignment for the CTE specimens as gages needed to be aligned perfectly with the *x* and *y* directions of the panel. Each gage was applied under a microscope, which enhanced the ability to align the gage on the alignment marks which were scratched into the surface of the specimen. Gages were also applied to the front and back of each specimen, nominally at the same location, so that a true strain average through the panel was obtained.

Transverse modulus specimens were prepared in a similar manner to the CTE specimens. However, transverse modulus measurements are not highly affected by minor gage misalignment, which is the same as a fiber misalignment. A deviation of 5° will only induce an error of less than 1% (Fig. 4-9) [24].

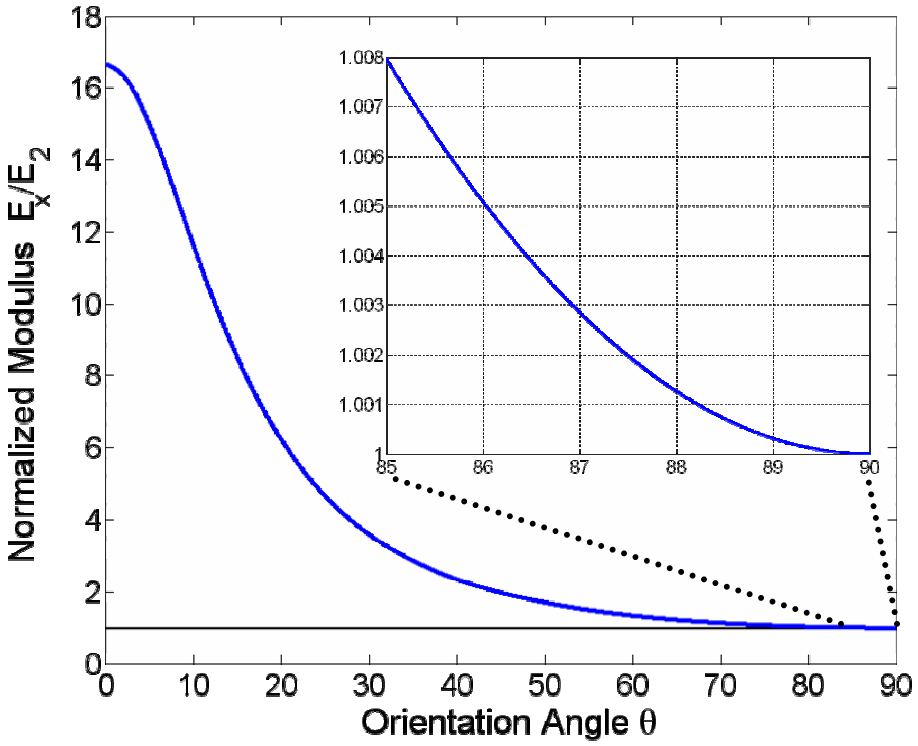

Figure 4-9. Transverse modulus misalignment errors

4.4.2 Gage Thermal Effects

As discussed in Section 4.1, thermal effects induced on the gage must also be considered when using strain gages. Figure 4-10 shows the thermally induced output, in terms of apparent strain, of the specific gages that were used on the tested specimens.

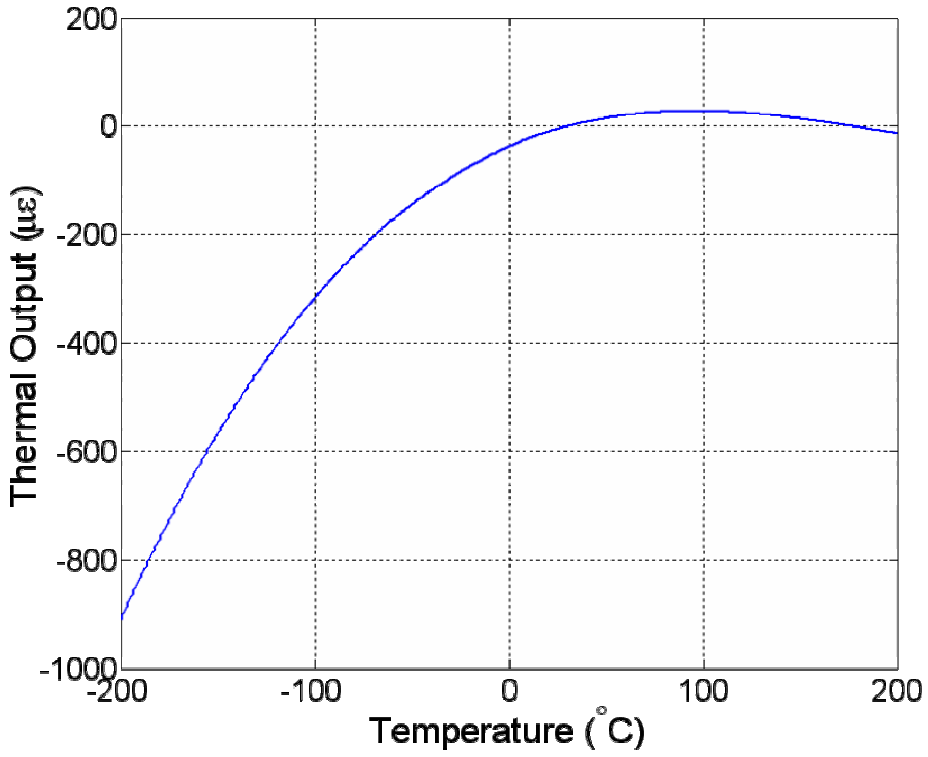

Figure 4-10. Gage thermal output

It can be seen that this gage is susceptible to thermal effects especially at cryogenic temperatures, where the thermal output of the gage can add almost -0.1% strain to the measured result. Due to this thermally induced strain from the gage, some form of temperature compensation must be employed when using strain gages over large temperature ranges.

CHAPTER 5
EXPERIMENTAL RESULTS

Specimens were first tested in the interferometer to obtain a reference point of strain at room temperature. These tests were then used in correlation with strain gage measurements to obtain the true strain on the surface of the composite specimens over a broad temperature range. With this data, the coefficient of thermal expansion and residual stress information within the panels as a function of temperature, as well as chemical shrinkage information could be determined. Separate tests also determined the transverse modulus, E_2, as a function of temperature in order to increase the knowledge base on the material behavior as a function of temperature.

5.1 Cure Reference Method

Each specimen that was produced was placed in the interferometer and its displacement information in both the *x* and *y* directions was documented with Polaroid film. Typical fringe patterns from each of the three types of layups are shown in Fig. 5-1. The displacement information, for each specimen, was converted to strain as shown in Chapter 3, and results are presented in Table 5-1 to 5-3. Recall that this measurement of strain is the true strain of the composite panels at 24°C and will be used in the next section to obtain accurate surface strain versus temperature data.

5.2 Surface Strain

As mentioned previously, strain gages were used to measure the strains over the desired temperature range of cure to cryogenic, and room temperature (24°C) was chosen as the reference temperature point. Strain measurements were zeroed out at 24°C and

Table 5-1: True strain reference on unidirectional (UNI) laminates at 24°C

Specimen	x-direction(με)	y-direction(με)
UNI-13-B2-02	≈0	-6955
UNI-13-02-03	≈0	-6500
UNI-13-02-05	≈0	-6824
UNI-13-03-02	≈0	-7220
UNI-13-06-04	≈0	-6890
Average	≈0	-6824
COV	---	3.77%

Table 5-2: True strain reference on "quasi-isotropic" (RLV) laminates at 24°C

Specimen	x-direction(με)	y-direction(με)
RLV-A1-01	-610	-190
RLV-02-02	-525	-197
RLV-03-03	-525	-220
RLV-05-04	-590	-230
Average	-562.5	-209.25
COV	6.78%	7.80%

Table 5-3: True strain reference on optimized angle ply (OAP) laminates at 24°C

Specimen	x-direction(με)	y-direction(με)
OAP-12-B3-01	787	-4920
OAP-12-03-02	820	-5250
OAP-16-04-01	919	-4950
OAP-16-02-02	1030	-5510
OAP-20-07-05	1033	-5250
Average	917.8	-5176
COV	12.5%	4.72%

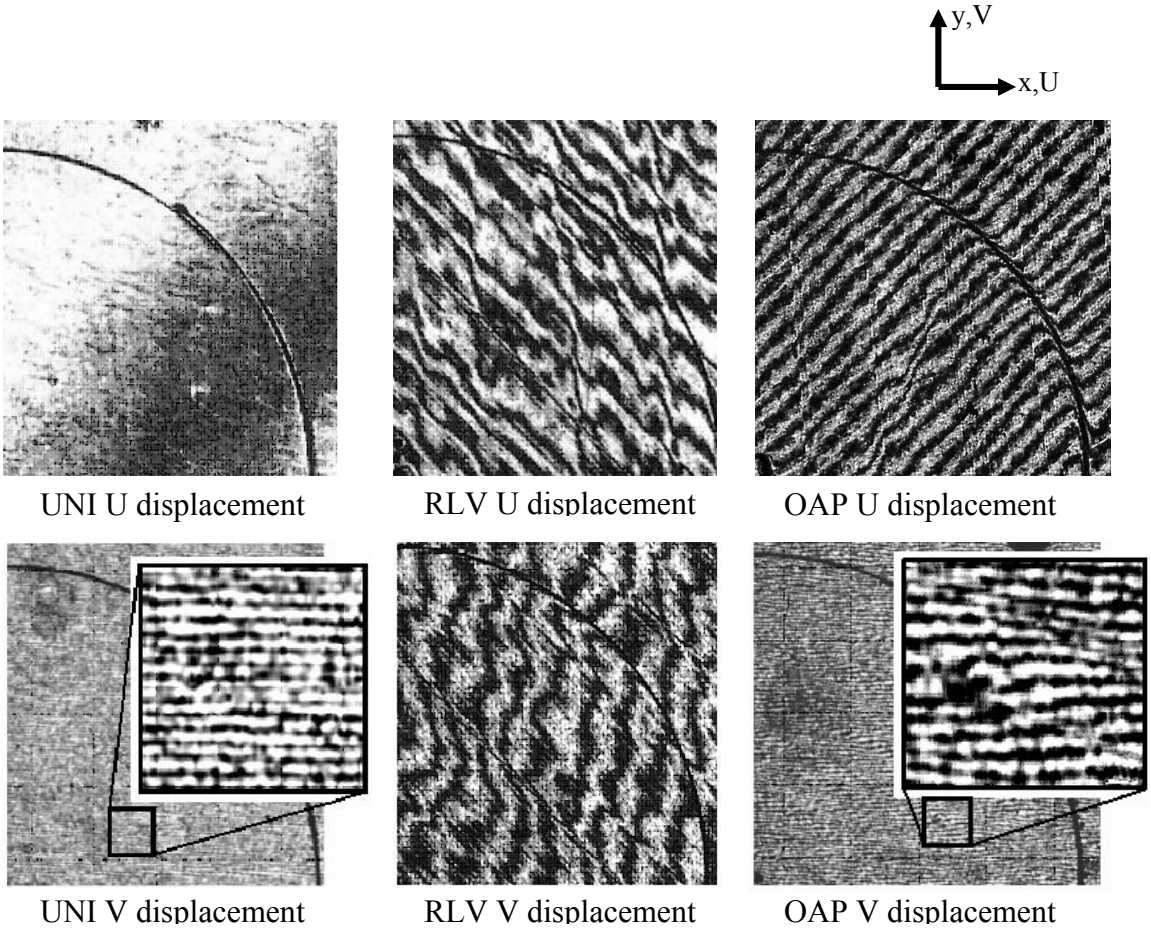

Figure 5-1. Typical fringe patterns of each type of tested layup

then recorded over the entire temperature range. The measured strain was the relative change in strain from the reference point to the specific temperature at which the measurement was taken. Since the reference point was chosen as 24°C, the relative change in strain information, obtained via strain gages at 24°C, was superimposed with the 24°C true strain measurement for each panel obtained via CRM. This allowed the generation of strain as a pure function of temperature for each composite panel. Figures 5-2 to 5-4 show the strain as a function of temperature for all the tested panels in each of the different layups. One can see good agreement between test runs, as evidenced by the overlap of the experimental data. However, to obtain a better statistical dataset, many

more specimens of each individual layup should be tested. It should be noted that the "quasi-isotropic" layup experiences strain values an order of magnitude smaller than the other two layups. This is purely due to the fact that the layup is highly constrained. Having plies in many directions inhibits the plies from deforming, thus reducing the total strain experienced by that layup. Also, note that strain in the *y-direction* is half of the strain in the *x-direction*. This is due to the layup of the panel, where there are twice as many plies in the *y-direction* as there are in the *x-direction.*

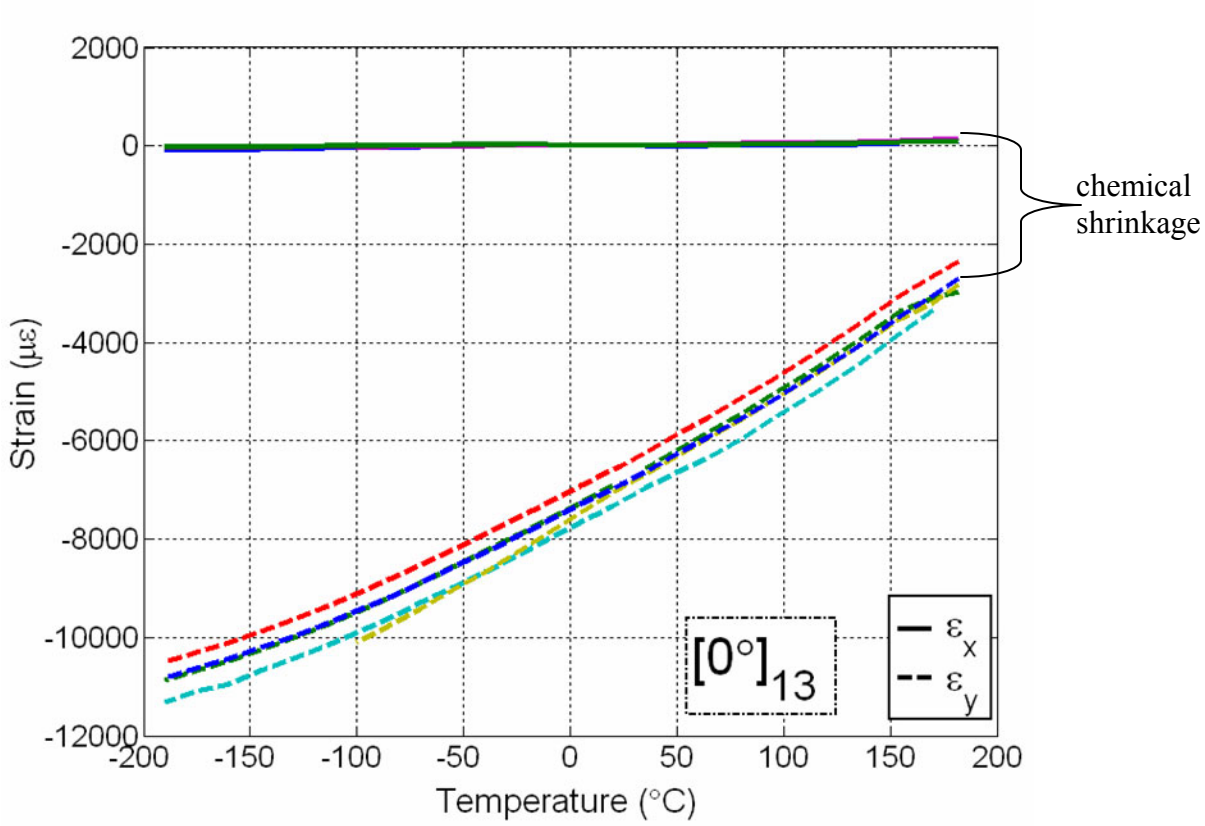

Figure 5-2. Unidirectional strain as a function of temperature, all tested specimens shown. Chemical shrinkage also shown

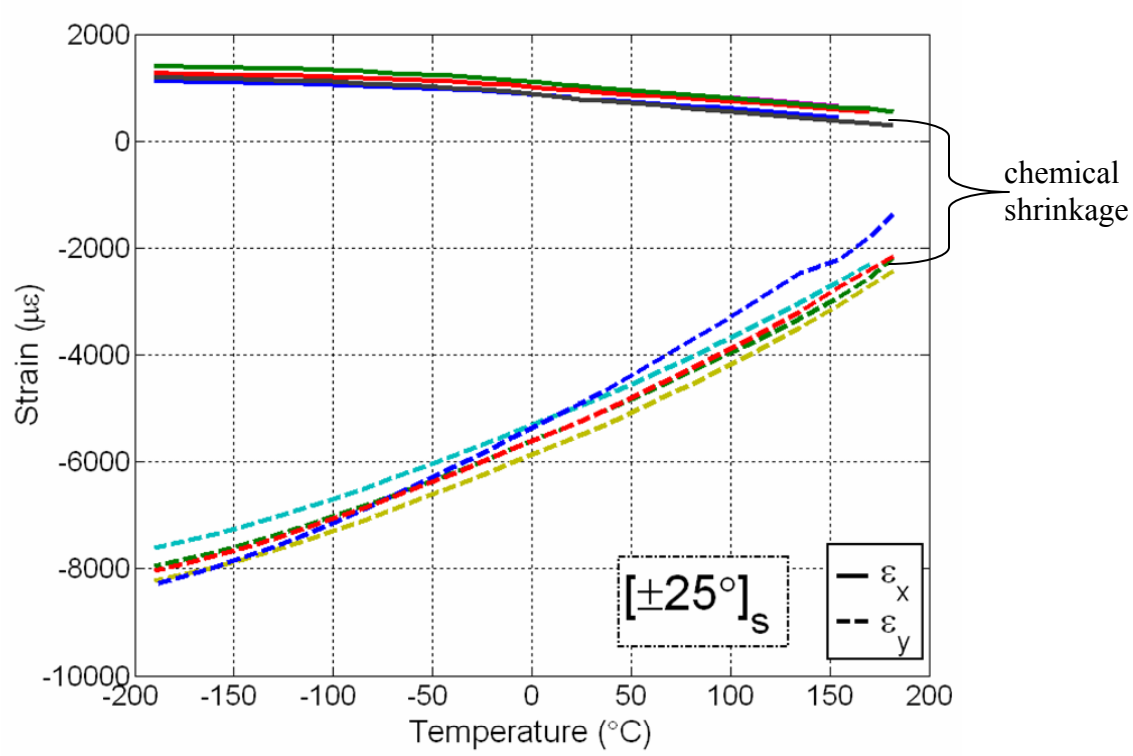

Figure 5-3. OAP strain as a function of temperature, all tested specimens shown

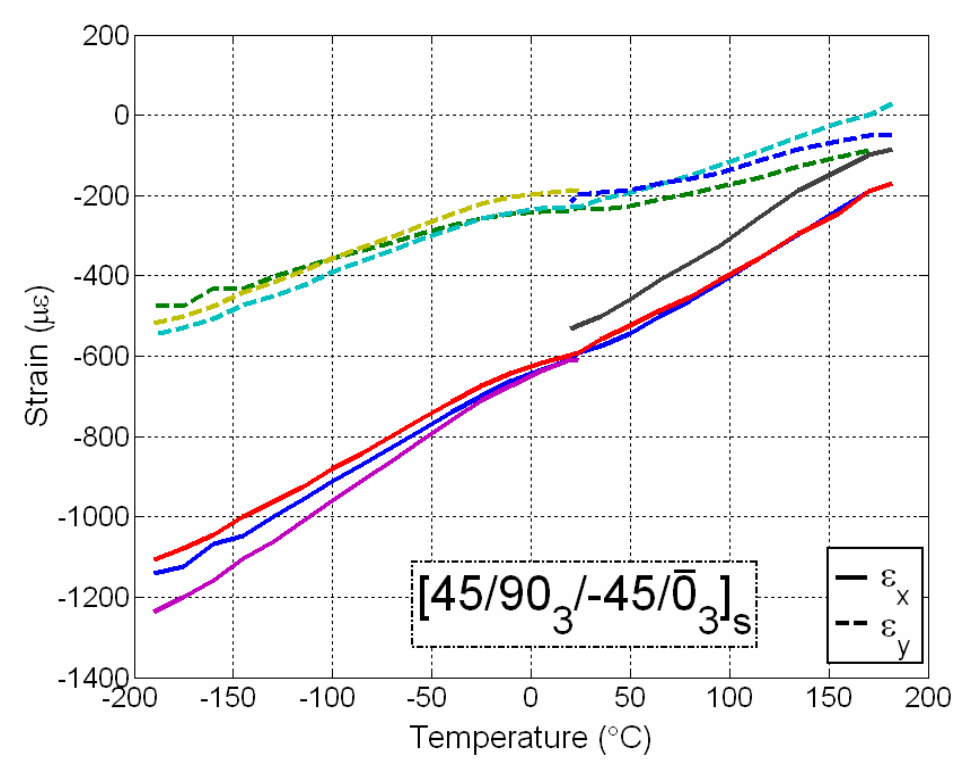

Figure 5-4. RLV strain as a function of temperature, all tested specimens shown

5.3 Chemical Shrinkage

Evident in Figures 5-2, 5-3, and 5-4 is the chemical shrinkage contribution to the total strain on the composite. Looking at the strain verses temperature data, it can be seen that the strains do not truly go to zero at the cure temperature of the composite specimens, as commonly assumed. The strain difference that exists at the cure temperature is the chemical shrinkage contribution. Recall that, in general, this is a permanent one-time phenomenon. Chemical shrinkage continues to occur at a degraded rate while the composite is subjected to elevated temperatures. However, the majority of the shrinkage occurs during cure. The average values of the chemical shrinkage on the panels are shown in Table 5-4 below.

Table 5-4: Chemical shrinkage strain on composite specimens

Specimen Type (# used)	x-direction (με)	Standard Deviation	Range	y-direction (με)	Standard Deviation	Range
UNI (5)	108	46.1	107	-2712.5	273.7	640
RLV (2)	-126.6	*	85.4	-9.25	*	77.04
OAP (3)	476.9	*	283.6	-2026.9	463.0	1071

* Not enough data to calculate

5.4 Coefficient of Thermal Expansion

Once the strain is known as a function of temperature, the coefficients of thermal expansion can then be calculated as a function of temperature. Using Eqs. (5-1) and (5-2) the instantaneous CTE in the *x* and *y* directions were approximated by a central difference scheme. The CTE is approximated at a point in the middle of two successive temperature data points; T_{+1} above the middle and T_{-1} below the middle.

$$CTE_x(T) = \frac{\varepsilon_x(T_{+1}) - \varepsilon_x(T_{-1})}{(T_{+1} - T_{-1})} \tag{5-1}$$

$$CTE_y(T) = \frac{\varepsilon_y(T_{+1}) - \varepsilon_y(T_{-1})}{(T_{+1} - T_{-1})} \tag{5-2}$$

The CTE information is show in Fig 5-5, and it can be seen that over the temperature range there appears to be a linear trend in both directions for each panel. Thus linear curve fits were applied to the unidirectional data to obtain the coefficient of thermal expansion in the *1* and *2* directions, α_1 and α_2, as a function of temperature.

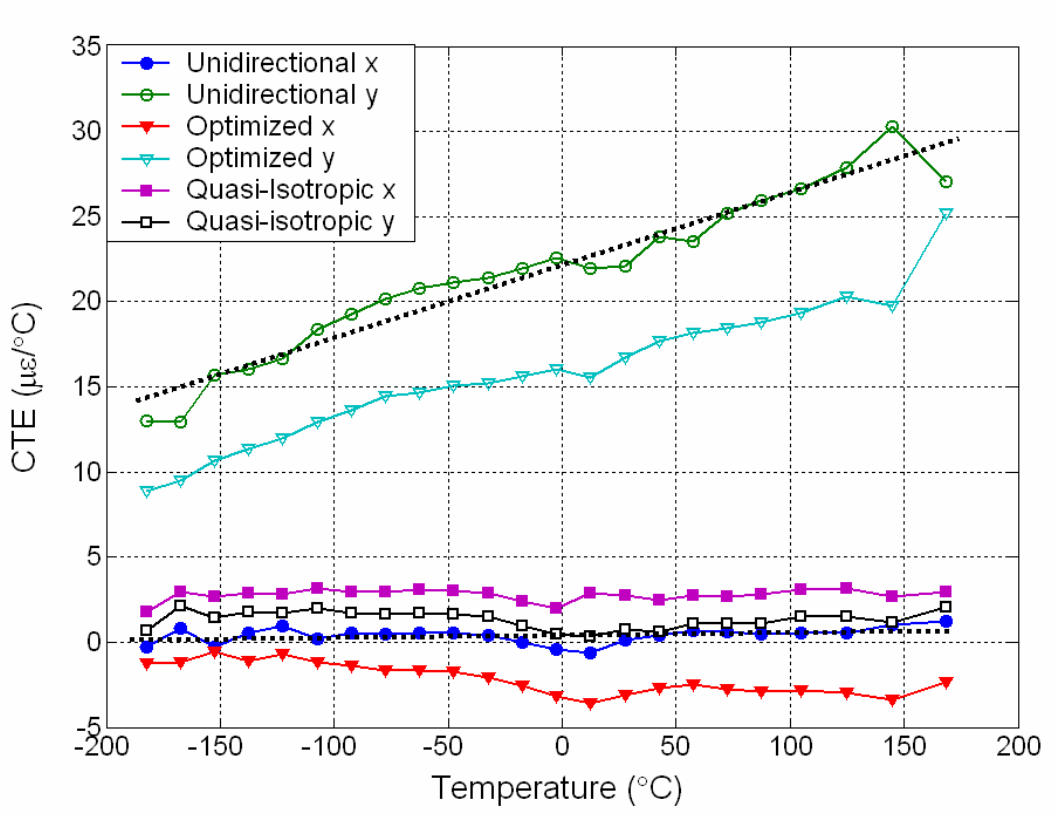

Figure 5-5. Coefficient of thermal expansion as a function of temperature

These fitted curves were used to improve analytical predictions and will be discussed in Chapter 6. The linear curves for unidirectional CTE are shown in Eqs. (5-3) and (5-4) below and are seen in Fig. 5-5 as dashed lines.

$$CTE_x^{UNI} = \alpha_1(T) = 0.0014 \cdot T + 0.4232 \ \frac{\mu\varepsilon}{^\circ C} \tag{5-3}$$

$$CTE_y^{UNI} = \alpha_2(T) = 0.0429 \cdot T + 22.167 \ \frac{\mu\varepsilon}{^\circ C} \tag{5-4}$$

Confidence intervals for each of the linear fits shown in Eqs. (5-3) and (5-4) is shown below in Table 5-5. Also shown are the Adjusted R^2 and RMSE values, which are representative of the goodness of the fits. The fit for the CTE in the fiber direction has a very poor R^2 value and a large confidence interval on the coefficients. This is because fiber expansion is typically a value close to zero. The data points used in the fit are extremely close to zero and have a large amount of scatter.

Table 5-5: Confidence intervals on fit of CTE data

$CTE_x^{UNI} = \alpha_1(T) = 0.0014 \cdot T + 0.4232 \ \frac{\mu\varepsilon}{^\circ C}$				$CTE_y^{UNI} = \alpha_2(T) = 0.0429 \cdot T + 22.167 \ \frac{\mu\varepsilon}{^\circ C}$			
$f(x) = a_1*T + a_0$				$f(x) = a_1*T + a_0$			
Coefficient		95% Upper	95% Lower	Coefficient		95% Upper	95% Lower
a_0	0.4232	0.6246	0.2217	a_0	22.17	22.65	21.68
a_1	0.001435	0.003378	-0.0005079	a_1	0.04288	0.04758	0.03819
Adjusted R^2		0.05819		Adjusted R^2		0.9423	
RMSE		0.4592		RMSE		1.11	

5.5 Transverse Modulus

The transverse modulus specimens and their dimensions are listed in Table 5-7. It can be seen that there is variation between test specimen dimensions, but the variation is acceptable with the given preparation methods. Each specimen's dimensions were obtained by averaging three measurements across the section of the specimen where the gage was to be applied. The measurements were taken with a micrometer, with a 0.001" resolution, prior to gage application so that the true cross sectional area of the specimen could be obtained. With the specimen dimensions known, the measured load vs. strain data could then be transformed to obtain the modulus of the material. The transverse modulus as a function of temperature for all tested specimens is shown in an average sense in Table 5-7 and individually in Fig. 5-6.

Table 5-6: Dimensions of E_2 specimens

Specimen	Width(in)	Thickness(in)
p2-2	0.090	0.987
p2-3	0.088	0.995
p2-4	0.0865	1.0025
p2-5	0.090	1.001
p2-7	0.083	0.995
p2-8	0.090	0.996
p2-9	0.089	1.001
p3-1	0.084	0.9995
p3-4	0.0866	1.0018
p3-5	0.087	1.001
COV	2.85%	0.48%

Table 5-7: Averages and COV of E_2 specimens

Temperature (°C)	Modulus (GPa)	COV (%)
-167.6882	12.4992	1.05
-145.1662	12.2427	0.87
-126.7379	11.9580	0.84
-102.9527	11.4554	0.80
-78.0718	10.7564	0.88
-52.9907	10.2190	0.98
-28.1746	9.8193	1.09
-3.2002	9.4364	1.13
22.8942	8.9941	1.04
48.2191	8.6328	1.16
73.8178	8.3893	1.33
99.4545	8.1829	1.48
125.2853	7.9310	1.50
151.2400	7.5062	1.73

As done for CTE measurements, the modulus data was curve fitted so that its temperature dependency could be included in analytical predictions. A nonlinear trend was seen in all tested specimens at temperature extremes and is seen in Fig. 5-6. Consequently, a 4th order polynomial fit was applied to the data and is shown in Eq. (5-5). A comparison between a linear fit is shown in Table 5-8 and Fig. 5-7 to justify the use of the 4th order fit over the linear fit.

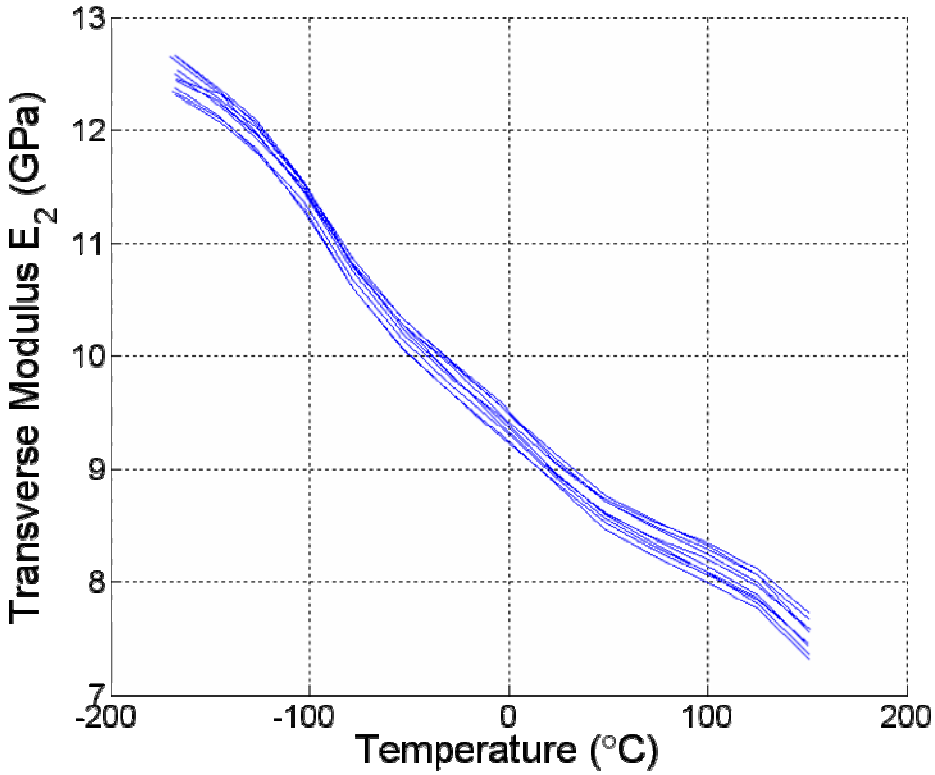

Figure 5-6. Modulus as a function of temperature for all tested specimens

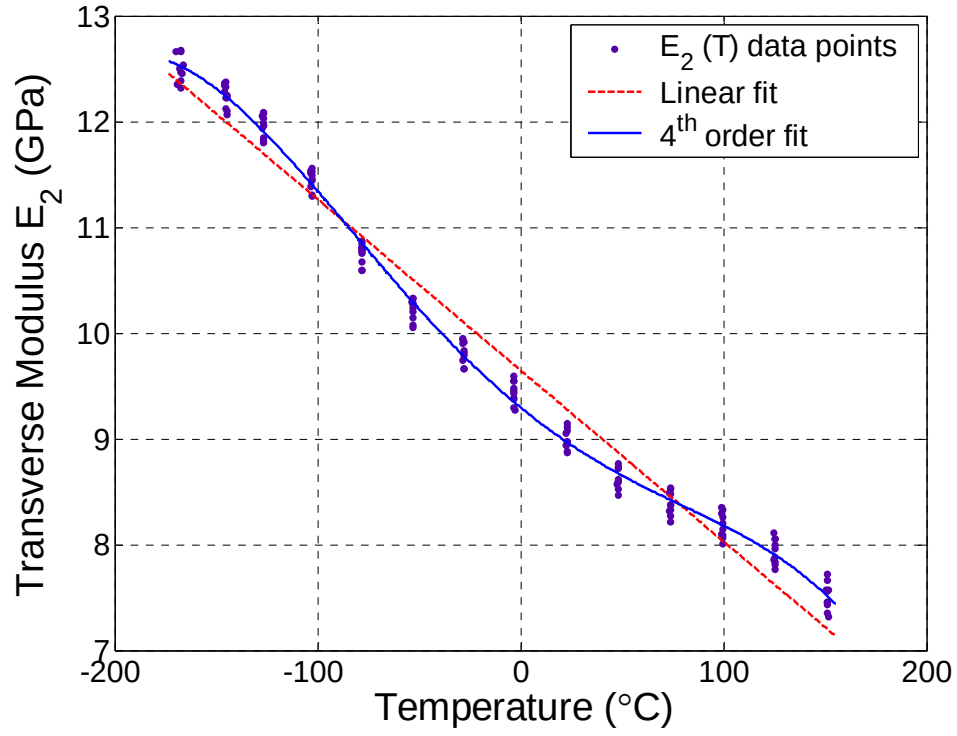

Figure 5-7. Modulus as a function of temperature fit comparison

Table 5-8: Confidence intervals on fit of E_2 data

Linear				4th Order			
$f(x) = a_1*T + a_0$				$f(x) = a_4*T^4 + a_3*T^3 + a_2*T^2 + a_1*T + a_0$			
Coefficient		95% Upper	95% Lower	Coefficient		95% Upper	95% Lower
a_0	9.65	9.693	9.607	a_0	9.298	9.335	9.261
a_1	-0.01618	-0.01576	-0.01661	a_1	-0.01572	-0.01521	-0.01623
Adjusted R^2		0.9755		a_2	6.125e-5	6.911e-5	5.339e-5
RMSE		0.2572		a_3	-9.267e-9	1.889e-8	-3.743e-8
				a_4	-1.486e-9	-1.176e-9	-1.797e-9
				Adjusted R^2		0.9951	
				RMSE		0.1153	

Table 5-8 shows a significant improvement on the adjusted R^2 value as well as the RMSE for the 4th order polynomial fit when compared to a linear fit. All tested transverse modulus specimens exhibited non-linear behavior over the tested temperature range. Therefore, the 4th order fit to the data, with T in ºC, was used and is show in Eq. (5-5). Note that the a_3 coefficient has been dropped due to the low confidence in that coefficient, presented in Table 5-8.

$$E(T) = -1.486e-9 \cdot T^4 + 6.125e-5 \cdot T^2 - 0.0157 \cdot T \; + \; 9.298 \;\; GPa \qquad (5\text{-}5)$$

5.6 Residual Stress

The residual stress within a ply can be obtained by analyzing the strain difference between what a ply is actually experiencing and what it would want to experience if the stresses bonding it to its neighboring plies were liberated. This liberated strain difference we define as the residual strain in the composite, and it is calculated based mainly on the assumption that the strain measured at the surface matches the strain at any point in the interior, as well as Kirchoff's hypothesis. Other assumptions that enable this calculation are discussed in Section 6.2. The residual strain was calculated for each ply orientation using Eq. (5-6) which takes the difference between a ply's unidirectional behavior and its behavior inside a laminate transformed by $[\tau_k]$ (Eq. 6-7) into the material coordinate

system (indicated by *1-2)*. The calculated residual strain and consequently residual stress in a laminate are a function of: stacking sequence, mechanical properties, thermal expansion properties, and chemical shrinkage.

$$\{\varepsilon_{res}\}_k = [\tau_k] \cdot \{\varepsilon_{lam}\} - \{\varepsilon_{uni}\} \tag{5-6}$$

After the residual strain has been determined, the residual stress can be defined by a constitutive relation, Eq. (5-7) that relates stress to strain through the use of the stiffness matrix of the composite panel, [Q], which is described in Chapter 6, Eq. (6-1).

$$\{\sigma_{res}\}_k = [Q]_k \{\varepsilon_{res}\}_k \tag{5-7}$$

The residual stress as a function of temperature in the direction transverse to the fibers is shown in Fig. 5-8 for the worst case ply orientation within the "quasi-isotropic" layup, as well as the optimized panel.

There are several important things to observe when looking at the initial analysis of the residual stress information shown in Fig. 5-8. Recall Fig. 5-4, which shows the surface strains on the RLV panel, and note that the strains on the RLV layup are an order of magnitude smaller than the other two panels. Typically, in composites low strains mean high stresses, which is evident in Fig. 5-8. Another thing to note, is that the worst case layer in the RLV layup has reached the failure strength (dashed horizontal line) of the matrix at LN_2 (-196 ºC) temperatures, a full 57 ºC above its intended operating LH_2 (-253 ºC) temperature. Stresses of this magnitude were what induced micro cracking within the matrix and ultimately were the root cause of the failure of the X-33 fuel tank. On the other hand, the residual stress in the optimized configuration is only half of the ultimate matrix strength at the extreme cryogenic temperatures. Also shown in Fig. 5-8 is the result that would be obtained if chemical shrinkage was not included in the surface

strain calculation. It can be seen that disregarding the chemical shrinkage contribution greatly underestimates the residual stresses within the laminate.

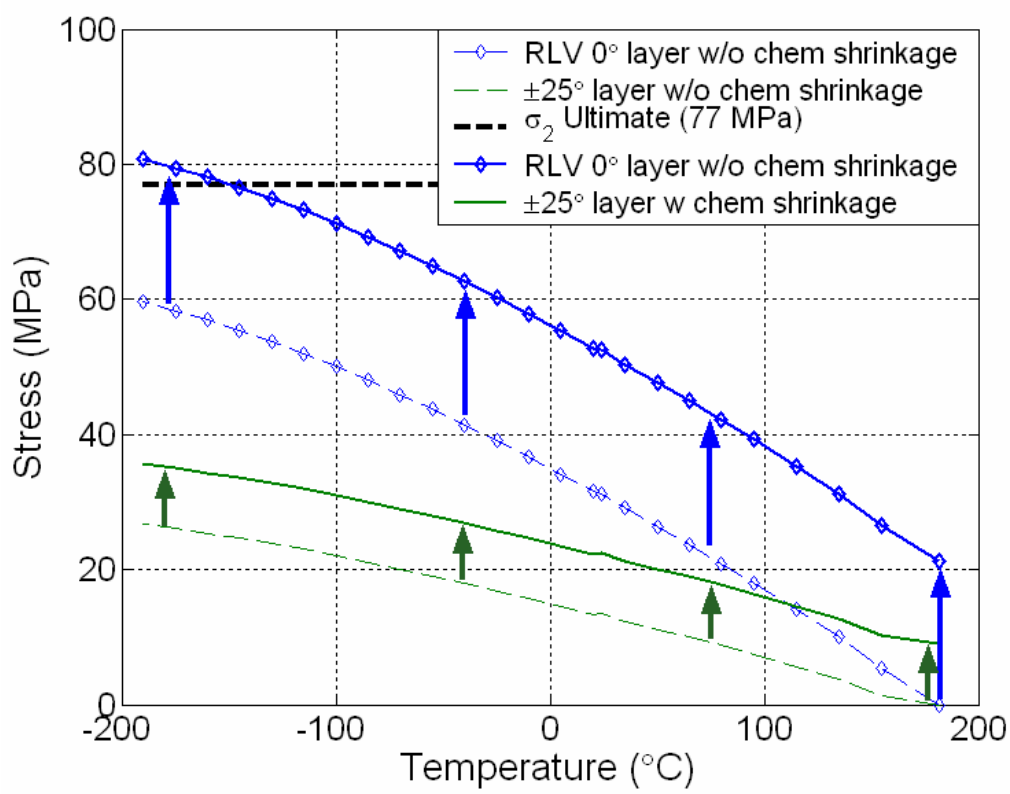

Figure 5-8. Residual stress as a function of temperature with chemical shrinkage

Transverse modulus is used in the calculation of [Q], and since it is known as a function of temperature, [Q] can be calculated as a function of temperature. Figure 5-9 shows the previous residual stress results from Fig. 5-8, represented by dashed lines, with results that allowed [Q] to vary as a function of temperature. The results show a significant increase in the residual stress values at the cryogenic temperatures (≈ 20%), with an expected crossover at room temperature.

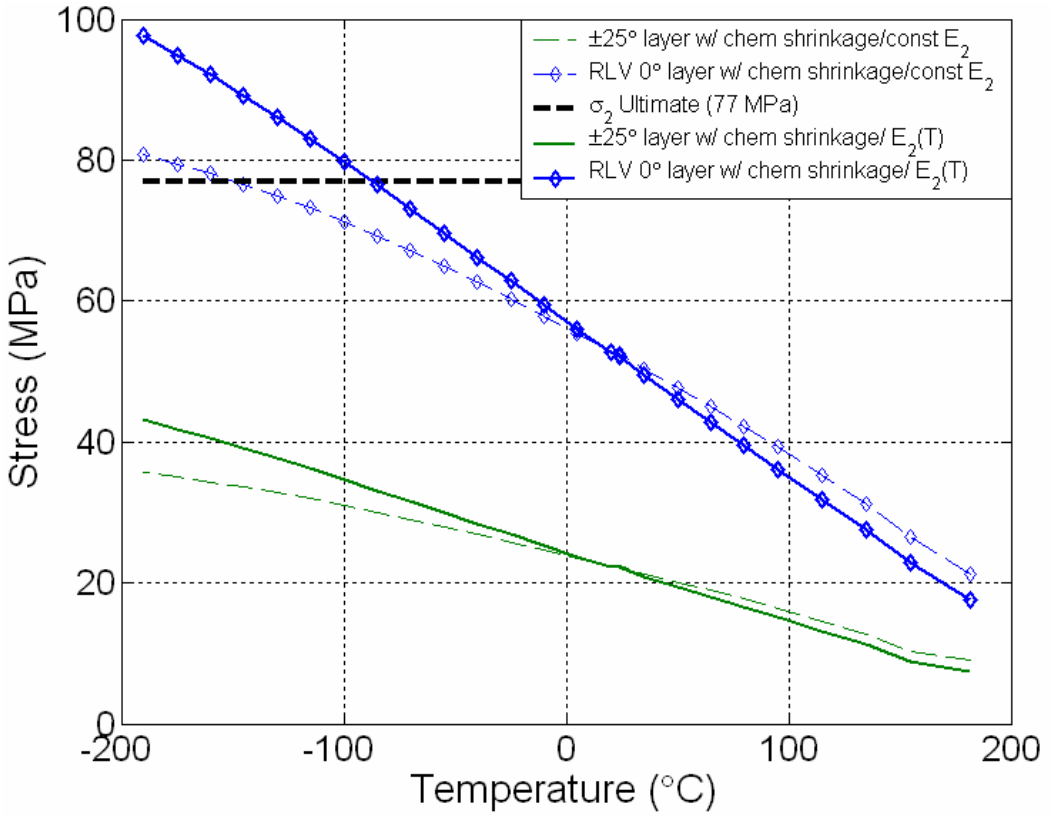

Figure 5-9. Residual stress as a function of temperature with temperature varying [Q]

CHAPTER 6
CLASSICAL LAMINATION THEORY

6.1 Purpose

Physical testing of graphite/epoxy material systems is currently a time intensive process. Each combination of fiber and epoxy behaves differently from any other combination. Specific combinations are chosen for a particular task that needs to be accomplished. To choose the correct material combination, designers need to be able to fully understand the physical behavior of the combination that they have chosen. Material behavior includes elastic properties such as Young's Modulus in the fiber and transverse directions, Shear Modulus, and Poisson's Ratio, as well as thermal expansion behavior. All of these properties are important in validating a chosen material system as a viable material to use.

To determine the behavior of a specific layup, currently one must construct that layup and subject it to a series of tests to obtain its thermal expansion properties and its mechanical behavior. An entirely new series of tests must be conducted for each layup of interest of a specific material system. This is a time consuming and expensive process. Thus there is a need for a method that can predict material behavior and characteristics of any layup in a short time at a minimum cost, and reasonable accuracy.

The analytical technique presented here is proposed as a method to predict the process induced strains on a composite panel based on a few simple tests carried out on unidirectional samples of the given material system. This means that the process of testing individual layups of a given material system to determine their behavior can be

eliminated. The behavior of a laminate with any ply orientation can be predicted with the information collected from the tests implemented on the unidirectional specimens.

6.2 Classical Lamination Theory Background

Classical Lamination Theory (CLT) is a commonly used predictive tool, which evolved in the 1960s, that makes it possible to analyze complex coupling effects that may occur in composite laminates. It is able to predict strains, displacements, and curvatures that develop in a laminate as it is mechanically and thermally loaded. The method is similar to isotropic plate theory, with the main difference appearing in the lamina stress-strain relationships. A rigorous explanation of the theory and formulation of CLT is shown in [13]. As with any analytical technique, some assumptions must be made in order to make the problem solvable.

1. The plate consists of orthotropic lamina bonded together, with the principal material axes of the orthotropic lamina oriented along arbitrary directions with respect to the *x*-*y* axes.
2. The thickness of the plate, *t*, is much smaller than any characteristic dimension.
3. The displacements *u*, *v*, and *w* are small compared to *t*.
4. The in-plane strains ε_x, ε_y, and γ_{xy}, are small compared with unity.
5. Transverse shear is negligible, $\gamma_{xz} = \gamma_{yz} = 0$, (plane stress in each ply).
6. Displacements u and v are assumed to be linear functions of the thickness coordinate *z* (no warping).
7. Assumptions 5 and 6 together define the Kirchhoff hypothesis.
8. Transverse normal strain ε_z is negligible.
9. Each ply obeys Hooke's Law.
10. The plate thickness is constant throughout the laminate.
11. Transverse shear stresses τ_{xz} and τ_{yz} vanish on the laminate surfaces $z = \pm t/2$.

These assumptions lay the foundation for the theory and enable prediction of composite laminate behavior. More detail will follow, so that one can understand the modifications made to the existing methodology.

6.3 Original Classical Lamination Theory

A program implementing CLT was written in MATLAB (Appendix) to calculate the strains in the given laminates as a function of temperature for comparison with our experimental results. Inputs include

- Combined constant temperature material properties of the lamina for the fiber and matrix (E_1, E_2, G_{12},ν_{12}, α_1, α_2)
- Stacking sequence and ply thickness
- Temperature difference from cure
- Mechanical loading conditions

On comparing of our experimental data to the analytically predicted results led to several noteworthy conclusions (Sections 6.3.1 and 6.3.2).

6.3.1 Optimized Angle Ply (OAP)

Results of the comparison for the $[\pm 25]_{nS}$ laminate are shown in Fig. 6-1. The first and most obvious is that in this specimen there is a significant relative error from the prediction and the experimental results. This relative error is approximately 20%-25%, and not considered a good prediction. Worth noting is that although the values of the prediction and the experiment do not coincide, their trends are virtually identical. The non-inclusion of chemical shrinkage is the man reason for the discrepancy between the prediction and the experimental results. Another key observation is that at the cure temperature of the composite, CLT predicts a zero strain state yet there is a significant amount of experimentally measured strain. This is due to the previously discussed chemical shrinkage phenomenon, which Classical Lamination Theory does not account for.

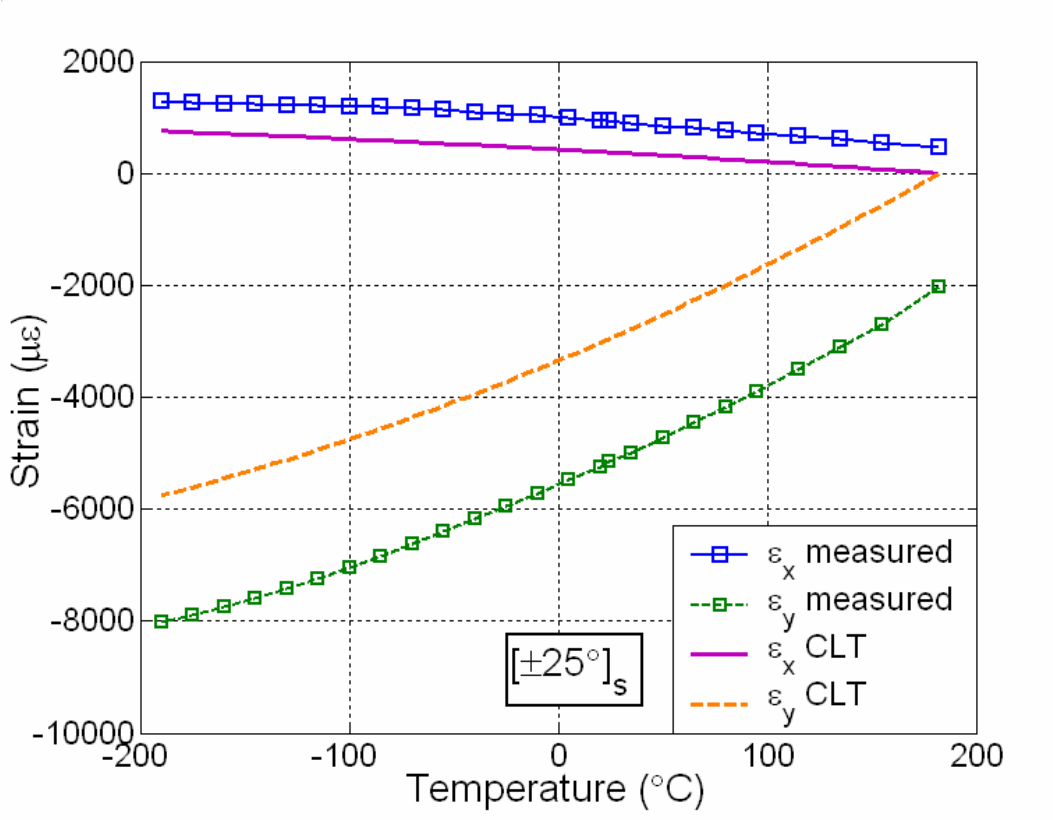

Figure 6-1. CLT vs. average of all experimental results for the OAP panel

6.3.2 "Quasi-isotropic" (RLV)

The results of the comparison for the $\left[+45/90_3/-45/\overline{0}_3\right]_S$ laminate are shown in Fig. 6-2. The results of the RLV laminate are similar to that of the OAP, but note that the strains are an order of magnitude smaller. As the name implies it acts as an almost-isotropic material, as it has plies in many directions. Having plies in many directions constrains the laminate heavily and thus low strains are seen. It can also be seen that in general the predicted and experimental data are in better agreement. The main reason for the better agreement is because of the properties of the layup. The more isotropic the laminate becomes, the more it begins to behave as a single isotropic layer rather than an assemblage of layers.

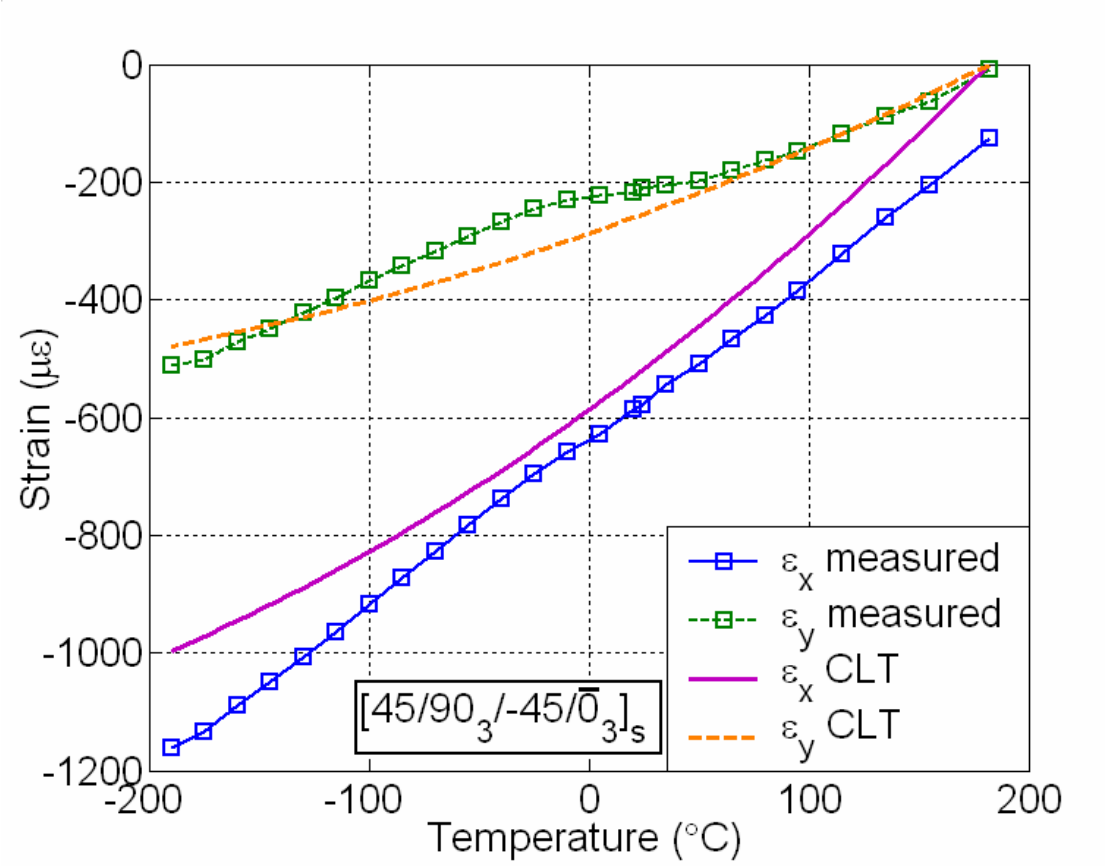

Figure 6-2. CLT vs. average of all experimental results for the RLV panel

6.4 Modified Classical Lamination Theory

Constant property CLT analysis is based on room temperature material properties. In order to improve the predictive capability of the model, material properties as a function of temperature were implemented in the program, as most mechanical properties tend to vary over large temperature ranges [25]. In addition to including the temperature dependent material properties, another method to increase the accuracy of the prediction is to include unidirectional chemical shrinkage information. Standard CLT analysis disregards the contribution of the chemical shrinkage of the epoxy, which can neglect a significant contribution to the overall behavior of the composite.

6.4.1 Temperature Dependent Material Properties

Temperature dependent CTE for the fiber, α_1, and transverse direction, α_2, as well as the transverse modulus, E_2, were implemented in the program. The ply stiffness matrix, $\boldsymbol{Q}$, which is shown in Eq. (6-1) contains the ply level material properties. Where E_1 and $E_2(T)$ are the effective Young's Moduli in the principal material coordinate directions (Fig. 6-3). The modulus transverse to the fiber direction is allowed to vary as a function of temperature within the model. Thus the compliance matrix must be redefined at each new temperature point. The CTE of the ply is also redefined at each new temperature point.

$$Q(T)=\frac{E_1}{E_1-E_2(T)\nu_{12}^2}\begin{bmatrix} E_1 & \nu_{12}E_2(T) & 0 \\ \nu_{12}E_2(T) & E_2(T) & 0 \\ 0 & 0 & G_{12} \end{bmatrix} \tag{6-1}$$

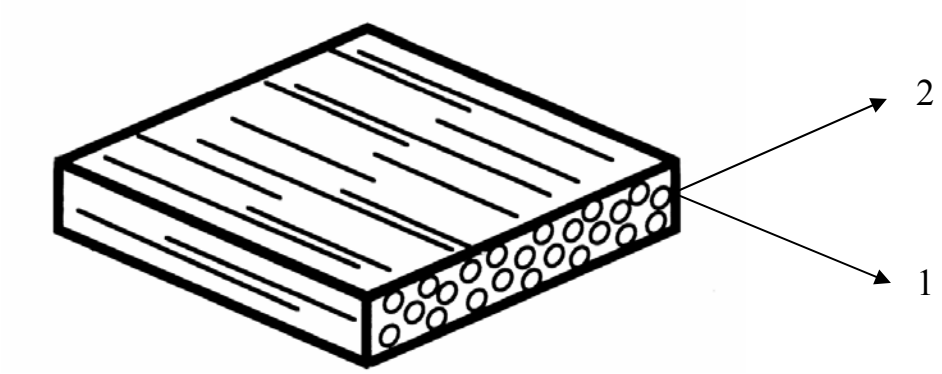

Figure 6-3. Principal material coordinates

A linear average, from cure temperature to the temperature of interest, was used at each successive temperature point in the analysis to calculate the average CTE's and modulus as shown in Eq. (6-2) and(6-3), where $\alpha_{1,2}(T)$ and $E_2(T)$ are Equations (5-3), (5-4) and (5-7) (which were obtained from experimental testing). Averaging the

mechanical properties, by integration, yields a more representative result of the true thermal variation in the property than does using an instantaneous value [26].

$$\alpha_{1,2avg}(T) = \frac{\int_{T_{cure}}^{T} \alpha_{1,2}(T)\,dT}{T - T_{cure}} \tag{6-2}$$

$$E_{2avg}(T) = \frac{\int_{T_{cure}}^{T} E(T)\,dT}{T - T_{cure}} \tag{6-3}$$

6.4.2 Chemical Shrinkage

Knowing that the chemical shrinkage is a permanent one-time phenomenon, in a thermoset polymer, and that it is similar to a thermal strain, one can include it in the calculation of thermal loads on the composite. As discussed previously, the unidirectional chemical shrinkage of the composite was obtained by calculating the strain present on the panel when returned to the cure temperature. This measurement is a representation of the chemical shrinkage an individual ply undergoes during the curing process. Knowing the value of the chemical shrinkage relative to the material coordinate system allows it to be included in CLT analysis.

6.4.3 Implementation

A governing relationship given by Eq. (6-4) establishes the connection between in-plane forces and moments to the mid-plane strains and curvatures on the laminate. This coefficient matrix is referred to as the *ABD* matrix of the laminate.

$$\begin{Bmatrix} N_x \\ N_y \\ N_{xy} \\ M_x \\ M_y \\ M_{xy} \end{Bmatrix} = \begin{bmatrix} A_{11} & A_{12} & A_{16} & B_{11} & B_{12} & B_{16} \\ A_{12} & A_{22} & A_{26} & B_{12} & B_{22} & B_{26} \\ A_{16} & A_{26} & A_{66} & B_{16} & B_{26} & B_{66} \\ B_{11} & B_{12} & B_{16} & D_{11} & D_{12} & D_{16} \\ B_{12} & B_{22} & B_{26} & D_{12} & D_{22} & D_{26} \\ B_{16} & B_{26} & B_{66} & D_{16} & D_{26} & D_{66} \end{bmatrix} \begin{Bmatrix} \varepsilon_x^0 \\ \varepsilon_y^0 \\ \gamma_{xy}^0 \\ \kappa_x \\ \kappa_y \\ \kappa_{xy} \end{Bmatrix} \tag{6-4}$$

For analysis, only the experimentally measured surface strains on the composite specimens were compared with the predicted strains from CLT. Knowing this, the *D* contribution of the *ABD* matrix can be disregarded. For symmetric laminates the *B* portion of the coefficient matrix is identically zero. This allows the reduction of Eq. (6-4) to the form of Eq.(6-5)

$$\{N\} = [A]\{\varepsilon_0\} \tag{6-5}$$

where the laminate extensional stiffness matrix , ***A***, is a representative stiffness of the entire laminate, obtained by summing each ply's contribution to the stiffness of the laminate as shown in Eq. (6-6)

$$A = t\sum_{k=1}^{NL}\left(\tau_k^{-1} Q_k R \tau_k R^{-1}\right) \tag{6-6}$$

where τ_k , Eq. (6-7), is the transformation matrix of the k^{th} layer and R , Eq. (6-8), is the Reuter Transformation Matrix which modifies the engineering/tensorial representation of the shear strain.

$$\tau = \begin{bmatrix} \cos^2\theta & \sin^2\theta & 2\cos\theta\sin\theta \\ \sin^2\theta & \cos^2\theta & -2\cos\theta\sin\theta \\ -\cos\theta\sin\theta & \cos\theta\sin\theta & \cos^2\theta - \sin^2\theta \end{bmatrix} \tag{6-7}$$

$$R = \begin{bmatrix} 1 & 0 & 0 \\ 0 & 1 & 0 \\ 0 & 0 & 2 \end{bmatrix} \tag{6-8}$$

Now that the stiffness matrix has been defined, one needs to define the constituents of the in-plane forces. The in-plane forces, {N}, are comprised of three major sections;

1. Forces due to imposed mechanical loads, $\{N^M\}$
2. Forces due to thermal expansion behavior of the laminate, $\{N^T\}$
3. Forces due to the chemical shrinkage of each ply as it cures, $\{N^C\}$

There were no applied mechanical loads during testing therefore there will be no contribution from the N^M term in the analysis. The contributions to the total in-plane forces for the thermal and chemical loading are shown below in Eqs. (6-9) and (6-10). Equation (6-10) allows the chemical shrinkage information from a unidirectional ply to be used to generate the chemical shrinkage experienced by a laminate of any given stacking sequence.

$$\left\{N^T\right\} = \left(T - T_{cure}\right)\left(\sum_{k=1}^{NL} \tau_k^{-1} Q_k R t_k \left\{\alpha_{avg}\left(T\right)\right\}\right) \tag{6-9}$$

$$\left\{N^C\right\} = \left(\sum_{k=1}^{NL} \tau_k^{-1} Q_k R t_k\right)\left\{\varepsilon_{uni}^{chemical}\right\} \tag{6-10}$$

It should be noted that the thermal and chemical loads are influenced by the thickness and orientation of the plies within the composite, which is shown by the existence of τ and t in the formulation of the loads.

Summing the two contributions, Eq. (6-11), leaves you with the total in-plane forces that are exerted on a panel while it experiences a temperature change from cure.

$$\left\{N\right\} = \left\{N^T\right\} + \left\{N^C\right\} = \sum_{k=1}^{NL} \tau_k^{-1} Q_k R t_k \left[\left(T - T_{cure}\right)\left\{\alpha_{avg}\left(T\right)\right\} + \left\{\varepsilon_{uni}^{chemical}\right\}\right] \tag{6-11}$$

By combining Eq. (6-5) and Eq. (6-11) the strain on the composite due to the influence of temperature and the chemical shrinkage of the epoxy can be obtained over the desired temperature range with Eq. (6-12).

$$\left\{\varepsilon\left(T\right)\right\}_{CLT} = \left[A\right]^{-1} \sum_{k=1}^{NL} \tau_k^{-1} Q_k R t_k \left[\left(T - T_{cure}\right)\left\{\alpha_{avg}\left(T\right)\right\} + \left\{\varepsilon_{uni}^{chemical}\right\}\right] \tag{6-12}$$

These modifications were implemented within CLT and the new results were compared with the experimentally obtained surface strain data, as will be shown in Sections 6.4.4 and 6.4.5. Each section will display the new prediction and the old predictions of CLT. A noticeable improvement on the prediction will be seen in Figures 6-4 and 6-5.

6.4.4 Optimized Angle Ply (OAP)

The results from the modified CLT analysis are shown in Fig. 6-4. Error bars representing a two-sigma confidence interval about each experimentally obtained data point are shown in the plot. It can be seen that the new prediction lies extremely close to the experimentally obtained data and well within the confidence interval. It can be seen that the prediction now shows a strain present at the cure temperature which is due to the inclusion of the chemical shrinkage information in the prediction.

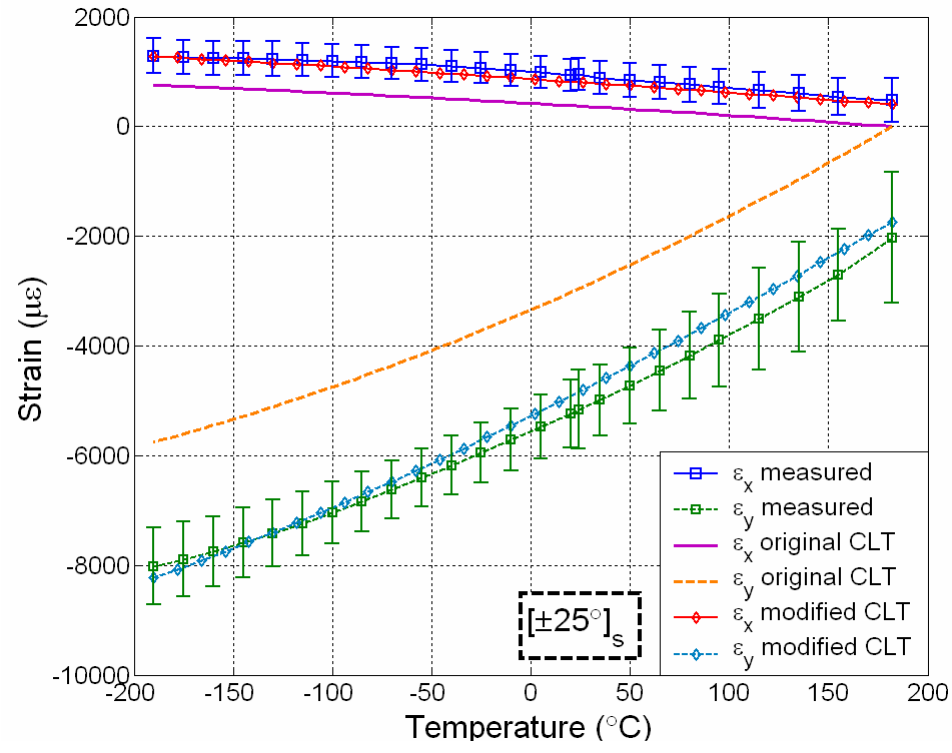

Figure 6-4. Modified CLT vs. experimental results for the OAP panel

6.4.5 "Quasi-Isotropic" (RLV)

The results from the modified CLT analysis are shown in Fig. 6-5. Error bars representing a two-sigma confidence interval about each experimentally obtained data point are shown in the plot. It can be seen that the new prediction lies extremely close to the experimentally obtained data and well within the confidence interval. It can be seen that the prediction now shows a strain present at the cure temperature which is due to the inclusion of the chemical shrinkage information in the prediction.

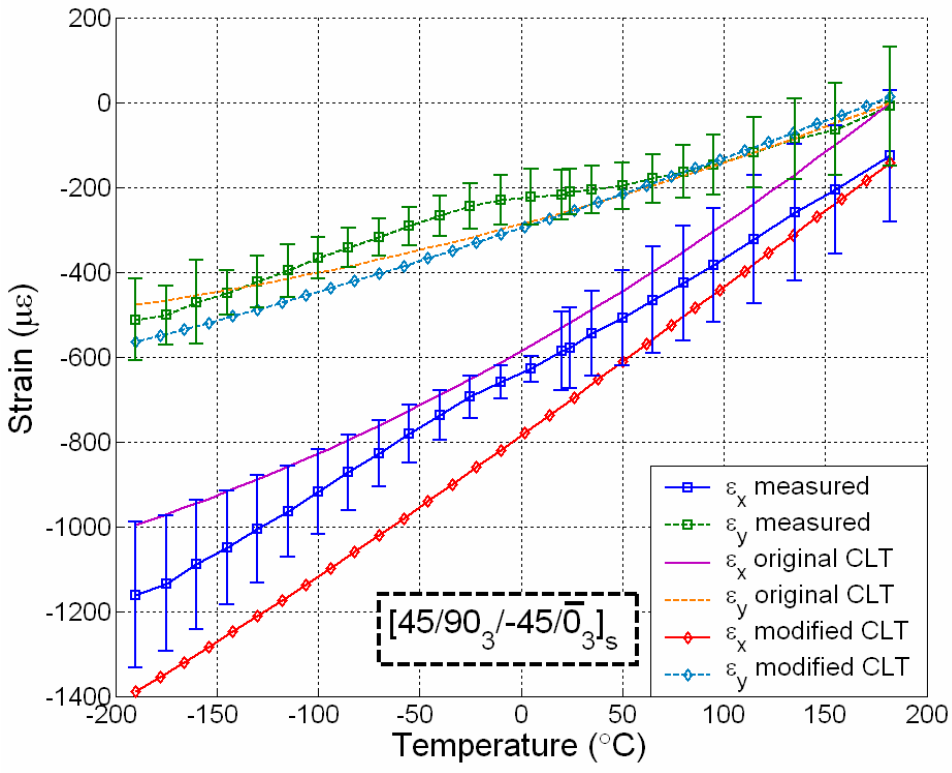

Figure 6-5. CLT vs. experimental results for the RLV panel

CHAPTER 7
UNCERTAINITY

For accurate quantitative results to be obtained, the uncertainty in the experimental results must be understood. Of critical importance are: error sources, repeatability, relative contribution of each error source, and the overall uncertainty in the final calculation.

7.1 Error Sources

There are many factors that can contribute errors to the experimentally obtained data shown in Chapter 5. Uncertainty quantities, in terms of bounds, for each factor are listed below:

- Equipment Resolution
  - Strain Gage ± 1 $\mu\varepsilon$ (assumed)
  - Temperature Diode ± 0.1 °C (manufacturers spec)
  - Load Cell ± 0.4 lbs (manufacturers spec)
  - Thickness measurement ± 0.001 in (assumed)
- Alignment
  - Strain Gage ± 2° (assumed)
  - Fiber Direction ± 2° (assumed)
  - Diffraction Grating ± 2° (assumed)

Analyzing what role each of these factors plays in the total uncertainty of the final measurement is crucial in being able to define the variability in measured results. Strain gauge and thickness measurement uncertainties result from the resolution of the measured output (one half the smallest readable increment). Load cell and temperature uncertainty are based upon manufacturer's specifications. Additional strain gage uncertainty arises from the uncertainty of alignment of a hand-placed gauge. Similarly,

misalignment of the layup or specimen preparation, as well as misalignment of the diffraction grating, will lead to further error sources.

Specifically for the material property measurements, the need arises to determine if the scatter in the data is purely experimental uncertainty, or if it is representative of the variability in that property. As was shown in Chapter 5, several transverse modulus specimens were tested, from several panels. The purpose of testing specimens from different panels was to obtain a measurement of the true variability in transverse modulus.

7.2 Analysis

Assuming that modulus is defined by Hooke's Law, Eq. (6-13), the uncertainty due to random errors, in transverse modulus, can be calculated using Eq. (6-14) [27, 28].

$$E = \frac{\sigma}{\varepsilon} = \frac{P}{A\varepsilon} = \frac{P}{wt\varepsilon} \tag{6-13}$$

$$\left(\frac{U_{E_2}}{E_2}\right)^2 = \left(\frac{U_P}{P}\right)^2 + \left(\frac{U_w}{w}\right)^2 + \left(\frac{U_t}{t}\right)^2 + \left(\frac{U_\varepsilon}{\varepsilon}\right)^2 \tag{6-14}$$

Equation (7-2) relates the relative uncertainty in the experimentally obtained E_2 to the relative uncertainties in the measured variables, where: U is the individual uncertainty contribution from each error source as indicated by subscripts, P (measured load), w (width), t (thickness), and ε (strain).

Evaluating Eq. (7-2) with nominal values (P, w, t, ε) and the uncertainties listed in the previous section:

$$\left(\frac{U_{E_2}}{E_2}\right)^2 = \left(\frac{0.4 \cdot lb}{200 \cdot lb}\right)^2 + \left(\frac{.001 \cdot in}{1.000 \cdot in}\right)^2 + \left(\frac{.001 \cdot in}{0.087 \cdot in}\right)^2 + \left(\frac{1\mu\varepsilon}{2000\mu\varepsilon}\right)^2$$

$$\left(\frac{U_{E_2}}{E_2}\right)^2 = \left(4.0E-6\right)_P + \left(1.0E-6\right)_w + \left(1.32E-4\right)_t + \left(2.5E-7\right)_\varepsilon$$

$$\frac{U_{E_2}}{E_2} = 1.17\%$$

This calculation shows that the uncertainty due to random errors in any given measurement of transverse modulus is 1.17%. Figure 7-1 shows data points for all specimens and an average curve of all specimens, with 1.17% error bars. It can be seen that most of the data points fall within 1.17% of the mean.

Note that the error obtained previously is only the random error in the measurements due to the limitations of equipment. There also exists a systematic or bias error. This error stems from the alignment uncertainties listed previously. Misalignment of the strain gage from the desired measurement direction, or the fibers in the specimen would cause a measurement to be offset from the true value. Fortunately, referring back to Fig. 4-9, it can be seen that misalignment of fibers or strain gages for transverse modulus tests, introduces less than 1% error with a 5° misalignment. This gives a greater confidence in the measured values. However, obtaining a concrete representation of the total error, a combination of the random and bias errors, is an ongoing task.

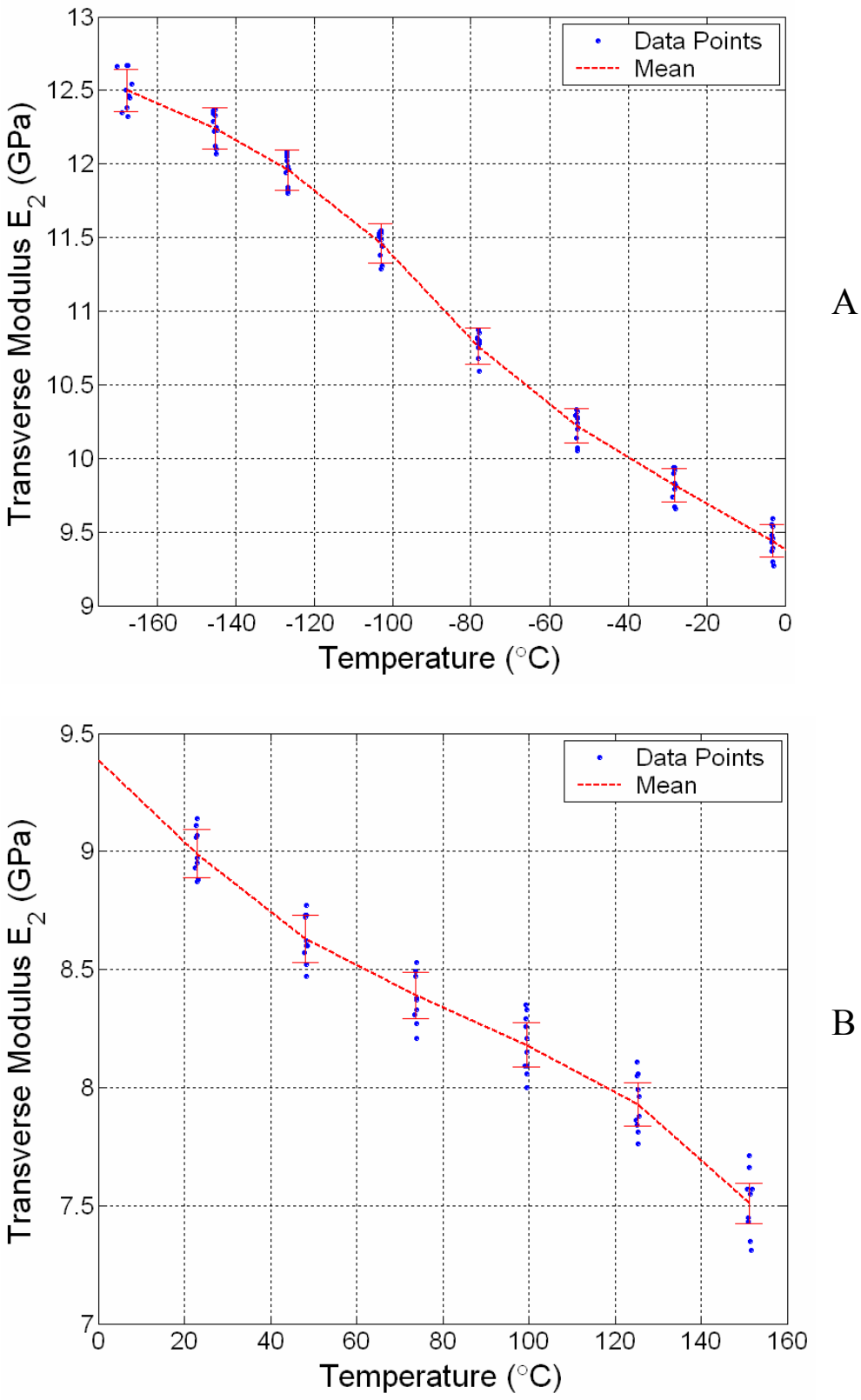

Figure 7-1. Transverse modulus with 1.17% error bars. A) Temperatures below 0°C. B) temperatures above 0°C.

7.2 Repeatability

Repeatability is also an important aspect of an experiment, which also is a representation of measurement errors. Figure 7-2 shows a single specimen that was subjected to two tests. The specimen was tested and removed from the testing setup; it was then replaced and retested. Slight differences can be seen between the individual runs, but overall the plot shows good agreement between the consecutive runs. Similar to previous results, a 4th order fit was applied to both curves. The fits from both curves are compared in Table 7-1 where good agreement between the coefficients and their confidence intervals is seen.

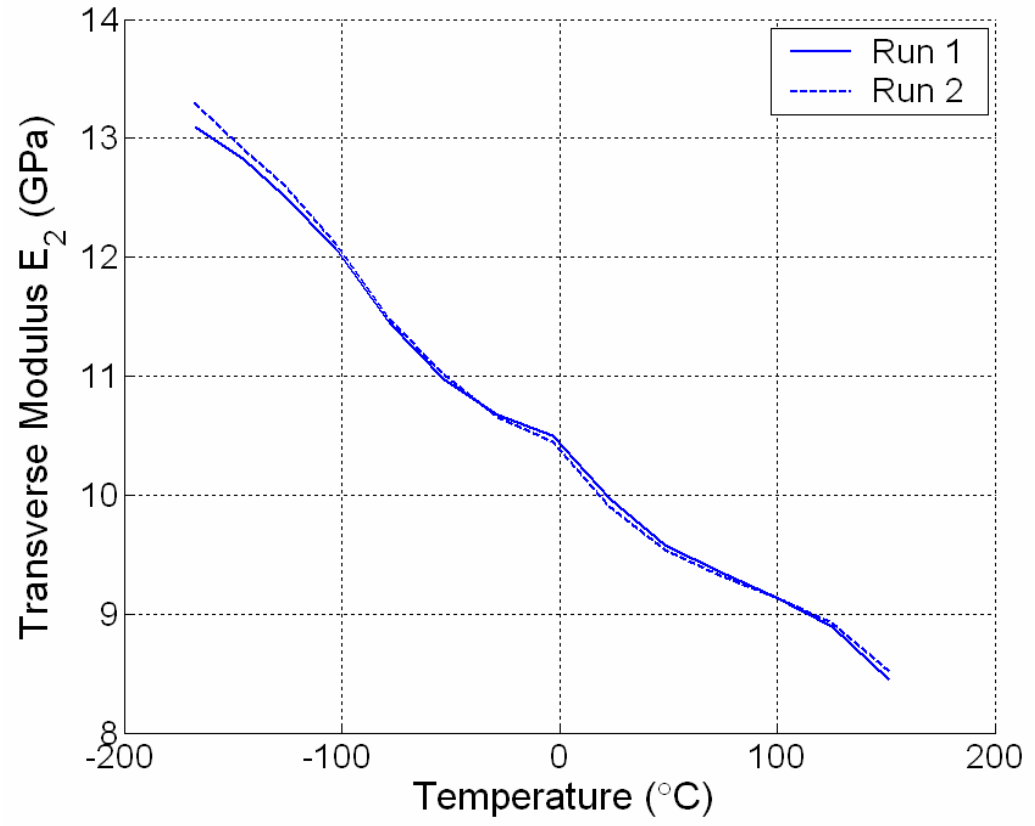

Figure 7-2. Repeated experiment on same specimen

Table 7-1: Confidence intervals and comparison on fits of E_2 repeat testing

4th Order Run 1				4th Order Run 2			
$f(x) = a_4*T^4 + a_3*T^3 + a_2*T^2 + a_1*T + a_0$				$f(x) = a_4*T^4 + a_3*T^3 + a_2*T^2 + a_1*T + a_0$			
Coefficient		95% Upper	95% Lower	Coefficient		95% Upper	95% Lower
a_0	10.25	10.36	10.14	a_0	10.21	10.31	10.11
a_1	-0.01376	-0.01218	-0.01534	a_1	-0.0142	-0.0128	-0.01561
a_2	3.897e-5	6.352e-5	1.443e-5	a_2	4.3e-5	6.467e-5	2.132e-5
a_3	-3.932e-8	4.74e-8	-1.261e-7	a_3	-2.689e-8	5.007e-8	-1.039e-7
a_4	-87.93e-9	8.842e-11	-1.847e-9	a_4	-7.824e-10	7.148e-11	-1.636e-9
Adjusted R^2		0.9959		Adjusted R^2		0.997	
RMSE		0.09796		RMSE		0.08681	

CHAPTER 8
CONCLUSIONS

Through our experiments we were able to implement easy and accurate methods to characterize thermal behavior as a function of temperature for our IM7/977-2 composite material system.

The Cure Reference Method was applied to several composite panels of varying stacking sequences. This technique allowed a reference point of absolute strain to be obtained for the panels at room temperature. This reference point was obtained for each specimen and recorded for further use.

Applying strain gages to the composite panels allowed the relative strain to be measured over a large temperature range. This relative strain was then transformed to an absolute strain over the temperature range by superimposing the absolute reference point obtained via the Cure Reference Method. Having an accurate representation of the strain as a function of temperature allowed the calculation of each panel's thermal expansion behavior, chemical shrinkage contributions, and residual stresses.

The residual stresses within the composite panels were quantified and compared. It showed that although the "quasi-isotropic" layup experienced low thermal expansion as well as low strains, it may not have been the best choice for the specific application of a cryogenic fuel tank. The layup is highly constrained, and thus produced large and undesirable stresses within the composite. Whereas the residual stresses in the layup originating from the optimization study, which yielded higher thermal expansion and strain behavior, stayed dramatically lower than the "quasi-isotropic" layup. This shows

that the "quasi-isotropic" layup was a poor choice, and stresses the importance of optimization studies. Also seen is that the chemical shrinkage of the epoxy can contribute a large quantity to the overall strain on a composite. Due to its magnitude, it is imperative that future measurements take this quantity into consideration.

Transverse modulus was also obtained as a function of temperature and the technique is easily adapted for measuring fiber direction modulus, E_1, Poisson's ratio, ν_{12}, and the shear modulus, G_{12}, all as functions of temperature. Specimens of the same dimension, yet different fiber orientation, can be fit into the current testing equipment. This allows for a single technique to be used to determine all necessary temperature dependent mechanical properties for a composite material system.

Modifications to the predictive capability of Classical Lamination Theory yielded markedly improved results. CLT is commonly used as a "ball park" technique, only to make sure that experimental results are in the right area, or to show if a particular material/configuration should be considered. Now with a small amount of effort given to accurately determine the chemical shrinkage of a material system as well as its mechanical properties as a function of temperature, the method can be used to predict the behavior of arbitrary layups with the same material system with very high confidence. This significantly decreases the need for time consuming testing of every new configuration within the material system that is being considered.

Future work should be done to obtain the remainder of the material properties as a function of temperature. As mentioned previously these properties are able to be obtained through the same methodology as the transverse modulus tests. Also more test panels of arbitrary stacking sequences should be produced and tested. These results

should be compared with the results from the modified form of CLT in order to test the robustness of the technique.

Random uncertainties were established and presented. Uncertainties due to misalignment of gages, fibers, and diffraction gratings could have an impact on the final properties measured and obtained. A rigorous error analysis was not completed, but is an ongoing task.

APPENDIX
CLASSICAL LAMINATION THEORY MATLAB CODE

Main Program: Backbone Operations

```
%CLT program

clear all close all clc
warning off
format short e

%Material Property Initialization

E1 = 149.92e+9;
v12 = .34198;
G12 = 4.77e+9;

plys = input('Enter the Number of plys you have: ');
t(1:plys)=1.242e-4;

for i = 1:plys
       disp(' ');
       disp(sprintf('Enter the fiber orientation of the #%d ply',i))
       theta(i) = input('');
end

unichemical=[108.6e-6;-2712.5e-6;0];
alpha1cure=0.678e-6;
alpha2cure=29.97e-6;
E2cure=6.0e9;

dT=0:-12:-372;
for j=1:32
a1=(0.0014e-6*(dT(j)+182) + 0.4232e-6 + alpha1cure)/2;
a2=(0.0429e-6*(dT(j)+182) + 22.167e-6 + alpha2cure)/2;
E2=(-0.0122e9*(dT(j)+182) + 9.4292e9 + E2cure)/2;
    for i = 1:plys

        % All Q & S calculations are stored in a 3D array for further
use (QANDS.m)

[Q,S,Qbar(:,:,i),Sbar(:,:,i),T(:,:,i)]=qands(E1,E2,G12,v12,theta(i));
        alphaglobal(:,i) = inv(T(:,:,i))*[a1;a2;0];
        alphaglobal(3,i) = 2*alphaglobal(3,i);
        chemicalglobal(:,i)=inv(T(:,:,i))*unichemical;
        chemicalglobal(3,i)=2*chemicalglobal(3,i);
    end

    [ABD,z,z0] = abd(t,Qbar,plys);
```

```
      %midplane strains & curvatures
      % disp(sprintf('Enter the loading conditions in a row vector
[Nx,Ny,Nxy,Mx,My,Myz]',i))
      % N_M = input('');
      N_M=[0 0 0 0 0 0];
      %Subroutine that calculates the thermal effects on the N's and
M's (THERMAL.m)
      [N_M_thermal]=thermal_chemical(Qbar,alphaglobal,chemicalglobal,dT
(j),plys,z0,z);

      N_M_total = N_M.' + N_M_thermal;
      e0_K = inv(ABD)*N_M_total;
      e0(:,1) = e0_K(1:3);
      K(:,1) = e0_K(4:6);

      %************************
      % GENERATES ALL Ex, Ey,exy
      %************************
      xstrain(1,1)=e0(1)+z0*K(1);
      ystrain(1,1)=e0(2)+z0*K(2);
      xystrain(1,1)=e0(3)+z0*K(3);
      for i = 2:plys+1
         xstrain(i,1)=e0(1)+z(i-1)*K(1);
         ystrain(i,1)=e0(2)+z(i-1)*K(2);
         xystrain(i,1)=e0(3)+z(i-1)*K(3);
         if abs(xystrain) < 1e-9
             xystrain(i,1)=0;
         end
      end

      for i = 1:plys+1
       e(:,i)=[xstrain(i,1);ystrain(i,1);xystrain(i,1)];
    end
      %************************************
      % GENERATES ALL Global & Ply stresses
      %************************************
      for i = 1:plys
        globalstresses(1:3,i)=Qbar(:,:,i)*(e(:,i)-
alphaglobal(:,i)*dT(j));
        globalstresses(4:6,i)=Qbar(:,:,i)*(e(:,(i+1))-
alphaglobal(:,i)*dT(j));
        plystresses(1:3,i)=T(:,:,i)*globalstresses(1:3,i);
        plystresses(4:6,i)=T(:,:,i)*globalstresses(4:6,i);
      end

      %*****************************************************
      % Plots and displays all needed values     (GRAPHICS.m)
      %*****************************************************
      %[thickness,strainthickness] =
graphics(z,z0,plys,globalstresses,plystresses,xstrain,ystrain,xystrain)
;
    format short g
    infor(j,1)=182 + dT(j);
    infor(j,2)=e(1,1)*1e6;
    infor(j,3)=e(2,1)*1e6;
end
```

Sub Program: Stiffness Calculations

```
%CALCULATES Q,Qbar, S, Sbar MATRICIES
%
function [Q,S,Qbar,Sbar,T]=qands(E1,E2,G12,v12,theta)

theta = theta*pi/180;
c = cos(theta);
s = sin(theta);

R = [1 0 0;0 1 0;0 0 2];                    %Rueter Transformation
Matrix
T = [c^2 s^2 2*c*s;s^2 c^2 -2*c*s; -c*s c*s c^2-s^2];%Transformation
Matrix

%****************
%Formulation of S
%****************
S11 = 1/E1;
S22 = 1/E2;
S66 = 1/G12;
S12 = -v12/E1;
S21 = S12;

S = [S11,S12,0;S21,S22,0;0,0,S66];

%****************
%Formulation of Q
%****************
Q = S^-1;

%***************************
%Formulation of Q-BAR & S-BAR
%***************************

Qbar = (T^-1)*Q*R*T*(R^-1);
Sbar = R*(T^-1)*(R^-1)*S*T;
```

Sub Program: ABD Assemblage

```
% CALCULATES THE ABD MATRIX OF THE PANEL
function [ABD,z,z0]=abd(t,Qbar,plys);

z0   = -sum(t)/2;
z(1) = z0+t(1);

%   cant use a zeroth row... so notation is offset by 1 number ..
%   for technically z_1 to z_(n+1) (same # of points)

for j = 2:plys
    z(j)=z(j-1)+t(j);
end

for i = 1:3
    for j = 1:3
        A(i,j) = Qbar(i,j,1)*(z(1)-z0);
```

```
        B(i,j) = Qbar(i,j,1)*(z(1)^2-z0^2)/2;
        D(i,j) = Qbar(i,j,1)*(z(1)^3-z0^3)/3;
        for k = 2:plys
            A(i,j) = A(i,j)+Qbar(i,j,k)*(z(k)-z(k-1));
            B(i,j) = B(i,j)+Qbar(i,j,k)*(z(k)^2-z(k-1)^2)/2;
            D(i,j) = D(i,j)+Qbar(i,j,k)*(z(k)^3-z(k-1)^3)/3;
        end
    end
end

ABD = [A,B;B,D];
```

Sub Program: Calculation of Thermo-Chemical Loading

```
% CALCULATES THE THERMAL AND CHEMICAL CONTRIBUTION TO THE RESULTANT
FORCES AND MOMENTS

function
[N_M_thermal]=thermal_chemical(Qbar,alphaglobal,chemicalglobal,dT,plys,
z0,z)

N_M_thermal = zeros(6,1);

N_M_thermal(1:3,1) = N_M_thermal(1:3,1) +
Qbar(:,:,1)*(alphaglobal(:,1)*(z(1)-z0)*dT+chemicalglobal(:,1)*(z(1)-
z0));
N_M_thermal(4:6,1) = N_M_thermal(4:6,1) +
Qbar(:,:,1)*(alphaglobal(:,1)*(z(1)^2-
z0^2)*dT/2+chemicalglobal(:,1)*(z(1)^2-z0^2)/2);

for i = 2:plys
    N_M_thermal(1:3,1) = N_M_thermal(1:3,1) +
Qbar(:,:,i)*(alphaglobal(:,i)*(z(i)-z(i-
1))*dT+chemicalglobal(:,i)*(z(i)-z(i-1)));
    N_M_thermal(4:6,1) = N_M_thermal(4:6,1) +
Qbar(:,:,i)*(alphaglobal(:,i)*(z(i)^2-z(i-
1)^2)*dT/2+chemicalglobal(:,i)*(z(i)^2-z(i-1)^2)/2);
end
```

Sub Program: Plotting

```
% PLOTTING FUNCTION

%*********************************************
% Plots and displays all needed values
%*********************************************

function [thickness,strainthickness] =
graphics(z,z0,plys,globalstresses,plystresses,xstrain,ystrain,xystrain)
;

%*********************************************************************
% sorts all stress/strains so they can be plotted
%*********************************************************************
j=1;
for i = 1:2:(plys*2-1)
```

```
      sigx(i)=globalstresses(1,j);
      sigx(i+1)=globalstresses(4,j);
      sigy(i)=globalstresses(2,j);
      sigy(i+1)=globalstresses(5,j);
      sigxy(i)=globalstresses(3,j);
      sigxy(i+1)=globalstresses(6,j);
      sig1(i)=plystresses(1,j);
      sig1(i+1)=plystresses(4,j);
      sig2(i)=plystresses(2,j);
      sig2(i+1)=plystresses(5,j);
      sig12(i)=plystresses(3,j);
      sig12(i+1)=plystresses(6,j);
      j=j+1;
end
%*********************************************************************
% Generates all thicknesses so that they can be plotted against the
stresses/strains
%*********************************************************************
thickness(1)=z0;
strainthickness(1)=z0;
m=2;
for i = 1:plys
      thickness(m)=z(i);
      thickness(m+1)=z(i);
      m=m+2;
end
[m,n]=size(thickness);
thickness=thickness(1:(n-1));

m=2;
for i = 1:plys
      strainthickness(m)=z(i);
      m=m+1;
end
strainthickness;
clc

figure(1);plot(sigx,thickness,'b-')
legend('Sigma X',0);ylabel('Thickness(mm)');xlabel('Stress(Pa)');
title('Stress through the thickness in the (X,Y) coordinate system')

figure(2);plot(sigy,thickness,'b-')
legend('Sigma Y',0);ylabel('Thickness(mm)');xlabel('Stress(Pa)');
title('Stress through the thickness in the (X,Y) coordinate system')

figure(3);plot(sigxy,thickness,'b-')
legend('Sigma XY',0);ylabel('Thickness(mm)');xlabel('Stress(Pa)');
title('Stress through the thickness in the (X,Y) coordinate system')

figure(4);plot(sig1,thickness,'b-')
legend('Sigma L',0);ylabel('Thickness(mm)');xlabel('Stress(Pa)');
title('Stress through the thickness in the (L,T) coordinate system')

figure(5);plot(sig2,thickness,'b-')
legend('Sigma T',0);ylabel('Thickness(mm)');xlabel('Stress(Pa)');
title('Stress through the thickness in the (L,T) coordinate system')
```

```
figure(6);plot(sig12,thickness,'b-')
legend('Sigma LT');ylabel('Thickness(mm)');xlabel('Stress(Pa)');
title('Stress through the thickness in the (L,T) coordinate system')

figure(7);plot(xstrain,strainthickness,'b-')
legend('x strain',0);ylabel('Thickness(mm)');xlabel('strain (m/m)');
title('Strain through the thickness in the (X,Y) coordinate system')

figure(8);plot(ystrain,strainthickness,'b-')
legend('y strain',0);ylabel('Thickness(mm)');xlabel('strain (m/m)');
title('Strain through the thickness in the (X,Y) coordinate system')

figure(9);plot(xystrain,strainthickness,'b-')
legend('shear strain',0);ylabel('Thickness(mm)');xlabel('strain
(m/m)');
title('Strain through the thickness in the (X,Y) coordinate system')
```

LIST OF REFERENCES

1. Final Report of the X-33 Liquid Hydrogen Tank Test Investigation Team, NASA George C Marshall Space Flight Center, Huntsville, AL 35812, May 2000.

2. Niu, X., "Process Induced Residual Stresses and Dimensional Distortions in Advanced Laminated Composites," PhD Dissertation, University of Florida, Gainesville, 1999.

3. Karkkainen R. L., "Empirical Modeling of In-Cure Volume Changes and Elasticity Development of Thermoset Polymers," M.S. Thesis, University of Tennessee, Knoxville, TN, 2000.

4. Nelson, D., Makino, A. and Hill, M., "Hole-within-a-Hole Method for Determining Residual Stresses," Proceedings of the Society for Experimental Mechanics, SEM X International Congress & Exposition on Experimental and Applied Mechanics, Costa Mesa, California, June 2004.

5. Joh, D., Byun, K. Y., and Ha, J., "Thermal Residual Stresses in Thick Graphite/Epoxy Composite Laminates-Uniaxial Approach," *Experimental Mechanics,* Vol. 33, No., pp. 70-76, 1993.

6. Kim, R. Y., and Hahn, H. T., "Effect of Curing Stresses on the First Ply-failure in Composite Laminates," *Journal Composite Materials,* Vol. 13, January, pp. 2-16, 1979.

7. Okabe, Y., Mizutani, T., Yashiro, S. and Takeda, N., "Detection of Microscopic Damages in Composite Laminates with Embedded Small-Diameter Fiber Bragg Grating Sensors," *Composites Science and Technology*, Vol. 62, No. 7-8, 2002, pp.951-958.

8. Daniel, I. M., Liber, T., and Chamis, C. C., "Measurement of Residual Strains in Boron/Epoxy and Glass/Epoxy laminates," *Composite Reliability, ASTM STP 580, American Society for Testing and Materials,* pp. 340-351, 1975.

9. Fenn, R. H., Jones, A. M., and Wells, G. M., "X-Ray Diffraction Investigation of Triaxial Residual Stresses in Composite Materials," Journal Composite Materials, Vol. 27, No. 14, pp. 1338-1351, 1993.

10. Ifju, P. G., Kilday, B. C., Niu, X. and Liu, S. C., "A Novel Means to Determine Residual Stress In Laminated Composites," Journal of Composite Materials, Vol. 33, No. 16, 1999.

11. Ifju, P. G., Niu, X., Kilday, B. C., Liu, S. C., Ettinger, S. M., "Residual Strain Measurement in Composites Using the Cure-referencing Method," Journal of Experimental Mechanics, Vol. 40, No. 1, pp. 22-30, March 2000.

12. Choi, S. and B.V. Sankar, "A Micromechanics Method to Predict the Fracture Toughness of Carbon Foam," 14th International Conference on Composite Materials, CD ROM proceedings, San Diego, California, July 2003, Paper # 1355.

13. Gibson, R. F., *Principles of Composite Material Mechanics*, McGraw-Hill Inc Publishers, New York, NY, 1994.

14. Qu, X., Venkataraman, S., Haftka, R.T., and Johnson, T.F., "Deterministic and Reliability-based Optimization of Composite Laminates for Cryogenic Environments," AIAA Journal, Vol. 41, No.10, pp.2029-2036.

15. Qu, X., Venkataraman, S., Haftka, R.T., and Johnson, T.F., "Reliability, Weight, and Cost Tradeoffs in the Design of Composite Laminates for Cryogenic Environments," 42nd AIAA/ASME/ASCE/AHS/ASC Structures, Structural Dynamics, and Materials Conference, AIAA-2001-1327.

16. Post, D., Han, B. and Ifju, P. G., "High Sensitivity Moiré: Experimental Analysis for Mechanics and Materials," Mechanical Engineering Series, Springer-Verlag, New York, NY, 1994.

17. Measurements Group, "Measurement of Thermal Expansion Coefficient," *Tech Note TN-513*, pp. 1-24. March 2005 http://www.vishay.com/brands/measurements_group/guide/indexes/tn_index.htm

18. Poussier, S., Hassan, R., Weber, S., "Adaptable Thermal Compensation System for Strain Gage Sensors Based on Programmable Chip," *Sensors and Actuators A: Physical*, Volume 119, Issue 2, 13 April 2005, Pages 412-417

19. Measurements Group, "Strain Gage Thermal Output and Gage Factor Variation with Temperature," *Tech Note TN-504*, pp. 1-17. March 2005 http://www.vishay.com/brands/measurements_group/guide/indexes/tn_index.htm

20. Cryogenic Technologies Group, Material Property References, National Institute of Standards and Technology. March 2005 http://www.cryogenics.nist.gov/NewFiles/material_properties.html

21. Moore, T., C., "Recommended Strain Gage Application Procedures for Various Langley Research Center Balances and Test Articles," NASA Technical Memorandum 110327.

22. "Standard Test Method for Tensile Properties of Polymer Matrix Composite Materials," *ASTM Standards D3039*, Vol. 15.03, pp 98-108.

23. Measurements Group, "Strain Gage Misalignment Errors," *Tech Note TN-511*, pp. 1-5. March 2005 http://www.vishay.com/brands/measurements_group/guide/indexes/tn_index.htm

24. Jones, R. M., *Mechanics of Composite Materials*, McGraw-Hill, New York, 1975

25. Johnson, T. F., Gates, T. S., "High Temperature Polyamide Materials in Extreme Temperature Environments," 42nd AIAA/ASME/ASCE/AHS/ASC Structures, Structural Dynamics, and Materials Conference, AIAA-2001-1214, April 2001.

26. Singer, T. N., "Comparison of Cure Reference Method and CLT for IM7/977-2 Laminates," AIAA Region II student conference, Memphis, TN, April 2004.

27. Holman, J. P., *Experimental Methods for Engineers*, 7th ed., McGraw-Hill, New York, 2001.

28. Coleman, H. W., Steele, W. G., *Experimentation and Uncertainty Analysis for Engineers*, 2nd ed., John Wiley & Sons, New York, 1999.

BIOGRAPHICAL SKETCH

William A. Schulz was born on March 10, 1980, in Miami, Florida. He lived in Weston, Florida and graduated from Western High School in June 1998. That summer he began his undergraduate career at the University of Florida (UF) in the department of Aerospace Engineering, Mechanics, and Engineering Science. In December of 2002 he graduated with honors with a Bachelor of Science degree in Aerospace Engineering. After receiving his bachelor's degree he continued his education at the UF in January 2003, in pursuit of a Master of Science degree from the newly merged Department of Mechanical and Aerospace Engineering. He served as a Graduate Research Assistant under Dr. Peter Ifju, director of the Experimental Stress Analysis Laboratory (ESALab). During his time in the ESALab, he conducted research on thermal variation of material properties of graphite/epoxy composites, primarily directed at use for cryogenic fuel tanks.